

Theoretical Modeling of Starburst Galaxies

L.J. Kewley, M.A. Dopita, R. S., Sutherland, C.A. Heisler¹, J. Trevena

Research School of Astronomy and Astrophysics, Australian National University

ABSTRACT

We have modeled a large sample of infrared starburst galaxies using both the PEGASE v2.0 and STARBURST99 codes to generate the spectral energy distribution (SED) of the young star clusters. PEGASE utilizes the Padova group tracks while STARBURST99 uses the Geneva group tracks, allowing comparison between the two. We used our MAPPINGS III code to compute photoionization models which include a self-consistent treatment of dust physics and chemical depletion. We use the standard optical diagnostic diagrams as indicators of the hardness of the EUV radiation field in these galaxies. These diagnostic diagrams are most sensitive to the spectral index of the ionizing radiation field in the 1-4 Rydberg region. We find that warm infrared starburst galaxies contain a relatively hard EUV field in this region. The PEGASE ionizing stellar continuum is harder in the 1-4 Rydberg range than that of STARBURST99. As the spectrum in this regime is dominated by emission from Wolf-Rayet (W-R) stars, this difference is most likely due to the differences in stellar atmosphere models used for the W-R stars. The PEGASE models use the Clegg & Middlemass (1987) planetary nebula nuclei (PNN) atmosphere models for the Wolf-Rayet stars whereas the STARBURST99 models use the Schmutz, Leitherer & Gruenwald (1992) Wolf-rayet atmosphere models. We believe that the Schmutz, Leitherer & Gruenwald (1992) atmospheres are more applicable to the starburst galaxies in our sample, however they do not produce the hard EUV field in the 1-4 Rydberg region required by our observations. The inclusion of continuum metal blanketing in the models may be one solution. Supernova remnant (SNR) shock modeling shows that the contribution by mechanical energy from SNRs to the photoionization models is $\ll 20\%$. The models presented here are used to derive a new theoretical classification scheme for starbursts and AGN galaxies based on the optical diagnostic diagrams.

1. Introduction

Observations of starburst galaxies can provide vital insights into the processes and spectral characteristics of massive star formation regions. In such regions the physical conditions are similar

¹deceased, 28 October 1999

to those that existed at the time of collapse and formation of galaxies in the early universe, and they can also provide an understanding of early galaxy evolution. The *Infrared Astronomical Satellite* (IRAS) made the key discovery of large numbers of infrared luminous galaxies, similar to those found by Rieke & Low (1972). Many of these are dominated by intense star formation (Lutz et al. 1996, 1998; Genzel et al. 1998; Veilleux et al. 1995; Veilleux, Kim & Sanders 1999) in which the luminosity of the young hot stars heats the surrounding dust, producing large amounts of infrared radiation.

The theoretical tools required to interpret the spectra of such galaxies are now available. For example, detailed stellar population synthesis models have been developed for both instantaneous and continuous starbursts and using these models, one is able to derive parameters such as the starburst age and metallicity from the continuous spectrum. In such models, the stellar initial mass function (IMF), star formation rate (SFR) and stellar atmosphere formulations are all adjustable initial parameters.

The emission line spectrum of the starburst provides constraints on the physical parameters for the ionized gas and the interstellar medium in general. In particular, the gas density, temperature and pressure can be derived directly from such observations, and the total rates of star formation can be estimated from the luminosity in the Balmer lines of hydrogen for the objects without large quantities of dust at least (*eg* Kennicutt (1998)). Using the ionizing UV radiation fields produced by stellar population synthesis models in conjunction with detailed self-consistent photoionization models such as MAPPINGS III (Sutherland & Dopita 1993) or CLOUDY (Ferland et al. 1998) we can now generate models for any H II region or starburst. In such models it is vital to include a self-consistent treatment of dust physics and the depletion of various elements out of the gas phase.

Since the nebular emission line spectrum is very sensitive to the hardness of the ionizing EUV radiation, optical line ratio diagnostic diagrams provide an important constraint on the shape of the EUV spectrum and these may also be used to estimate the mean ionization parameter and metallicity of the galaxies. Such optical diagnostic diagrams were first proposed by Baldwin, Phillips, & Terlevich (1981) to classify galaxies into starburst or AGN type, since AGN have a much harder ionizing spectrum than hot stars. The classification scheme was revised by Osterbrock & de Robertis (1985) and Veilleux & Osterbrock (1987), hereafter VO87. These revised diagnostics are used here. For both schemes, the line diagnostic tools are based on emission-line intensity ratios which turn out to be particularly sensitive to the hardness of the EUV radiation field.

In an earlier paper (Dopita et al. 2000), we theoretically recalibrated the extragalactic H II region sequence using these line diagnostic diagrams and others, in order to separate and quantify the effects of abundance, ionization parameter and continuous vs. instantaneous burst models. The theoretical H II region models were generated by the MAPPINGS III code which uses as input the EUV fields predicted by the stellar population synthesis models PEGASE v2.0 (Fioc & Rocca-Volmerange 1997) and STARBURST99 (Leitherer et al. 1999). Dust photoelectric heating and the gas-phase depletion of the heavy elements were treated in a self-consistent manner. This work found

that the high surface brightness isolated extragalactic H II regions are in general excited by young clusters of OB stars, and that, in this case, the ionizing EUV spectra and H II region emission line spectra predicted by the PEGASE and STARBURST99 codes are essentially identical.

For starburst galaxies, in which the starburst has a luminosity comparable to the luminosity of the host galaxy, the situation is rather different. In these objects, intense star formation is likely to continue over at least a galactic dynamical timescale, and therefore the assumption of a continuous rather than an instantaneous burst of star formation would be more accurate. As a consequence, the assumptions which go into the theoretical stellar mass loss formulations and evolutionary tracks are likely to play a much more important role in the modeling. Furthermore, for starbursts continued for more than a few Myr, the Wolf-Rayet (W-R) stars can play an important part in determining both the intensity and shape of the EUV spectrum. For the W-R stars, the uncertain assumptions made about the stellar lifetimes, wind mass-loss rates, the velocity law in the stellar wind, and the atmospheric opacities play a critical role in determining the spectral shape and intensity of the emergent EUV flux predicted by theory.

In this paper, we present new grids of theoretical models (based on the assumption of continuous star formation) which again combine H II region models generated by the MAPPINGS III code with input EUV fields given by the stellar population spectral synthesis models PEGASE 2 and STARBURST99. These models are used in conjunction with our large observational data set described in Kewley et al. (2000a) and Kewley et al. (2000b) to place new *observational* constraints on the shape of the EUV ionizing radiation field. Since the two stellar population spectral synthesis codes provide a wide choice of stellar mass loss formulations, evolutionary tracks and stellar atmospheric transfer models, they provide strikingly different predictions about the shape and intensity of the EUV field as a function of stellar age. In this paper, we use these to separate and quantify the effects of the stellar atmospheric models and the evolutionary tracks used on the optical diagnostic diagrams. In particular, we will show that the models which give the hardest EUV spectrum below the He II ionization limit, but which have relatively few photons above this limit, provide the best empirical fit to the distribution of starburst galaxies on the optical line ratio diagnostic diagrams. These new observational constraints should prove very helpful to theoreticians modeling the late stages of stellar evolution in massive stars.

This paper is structured as follows. Our observational comparison sample is described in Section 2. The stellar population synthesis models used to calculate the EUV ionizing radiation field are presented in Section 3. Our theoretical starburst models were produced using the photoionization and shock code MAPPINGS III and are described in Section 4. Wolf-Rayet emission in our sample of starburst galaxies is discussed in Section 5 and the effect of continuum metal opacities on the EUV ionizing continuum is discussed in Section 6. A new theoretical classification scheme for starbursts and AGN is presented in Section 7 and our main conclusions are summarised in Section 8.

2. The Observational Comparison Sample

We have selected a large sample of 285 warm IRAS galaxies covering a wide range of infrared luminosities. The warm selection criterion ensures that our sample contains galaxies with either concentrated star formation (Armus, Heckman, & Miley 1989, 1990), AGN (Miley, Neugebauer, & Soifer 1985), or in many cases, a combination of the two.

Our sample has been selected from the catalogue by Strauss et al. (1992) and consists of all objects south of declination $\delta = +10^\circ$ with the additional following criteria;

1. Flux at $60 \mu\text{m} > 2.5 \text{ Jy}$ with moderate or high quality detections at 25, 60 and $100 \mu\text{m}$
2. Redshift $< 8000 \text{ km s}^{-1}$ for $\log(L_{\text{FIR}}) < 11$ and $< 30000 \text{ km s}^{-1}$ for $\log(L_{\text{FIR}}) > 11$
3. Galactic latitude $|b| > 15^\circ$, and declination $\delta < +10^\circ$
4. Warm FIR colours; $8 > F_{60}/F_{25} > 0.5$ and $2 > F_{60}/F_{100} > 0.5$

where F_{25}, F_{60} and F_{100} are the IRAS fluxes at 25, 60 and $100 \mu\text{m}$ respectively. These selection criteria ensure that the galaxies in the sample are well-resolved, and that the sample has a large dynamical range in luminosity, so that luminosity dependent effects can, in principle, be investigated.

High resolution (50 km s^{-1} at $H\beta$) optical spectra with useable $S/N (> 3\sigma)$ ratios were obtained for 225 of the galaxies in our sample. Spectra were obtained in the red and blue wavelength ranges using the Double Beam Spectrograph on the Mount Stromlo and Siding Springs 2.3m telescope. These selection criteria and the full details of our observations are discussed in detail in Kewley et al. (2000a) and Kewley et al. (2000b). All 225 objects were classified into AGN, starburst and LINER types using new theoretical classification lines on the Veilleux & Osterbrock (1987) (hereafter VO87) diagnostic diagrams. We found 157 starburst galaxies using the VO87 diagrams and semi-empirical classification scheme which provide the primary observational comparison for the starburst spectral modeling presented here.

We believe there is little contamination by obscured AGN in this starburst sample for two reasons. Firstly, in Kewley et al. (2000a), we have shown that the optical diagnostic diagrams are extremely sensitive to the presence of an AGN. An AGN which contributes only 20% to the optical emission increases the line ratios sufficiently that it would be classified as an AGN. Secondly, we found very few starburst galaxies with warm colors ($\sim 4 < F_{60}/F_{25} < 8$). Since warm colors usually mean that the galaxy is energetically dominated by an AGN we can conclude that the fraction of obscured AGN in our starburst galaxies must be low. These results are consistent with the infrared studies of Veilleux, Kim & Sanders (1999) and Genzel et al. (1998), who showed that ultraluminous infrared galaxies classified as starbursts also show a lack of an energetically important AGN.

3. Stellar Population Synthesis Models

The models we have utilized are described in detail in Dopita et al. (2000), and we describe them again briefly here. We have used both the PEGASE 2 and STARBURST99 codes to model the starbursts in our sample. The PEGASE 2 code uses the Lejeune, Cuisinier & Buser (1997) grid of atmospheres covering the entire Hertzsprung-Russell diagram (HRD) plus Clegg & Middlemass (1987) planetary nebula nuclei (PNN) atmospheres for stars with high effective temperatures ($T > 50000$ K) (hereafter known as the Clegg & Middlemass atmospheres). The Lejeune, Cuisinier & Buser (1997) grid (hereafter called the Lejeune grid) is derived from three sets of atmosphere calculations, the bulk being the Kurucz (1992) models with smaller specialized cool star models by Fluks et al. (1994) and Bessell et al. (1989, 1991). Lejeune, Cuisinier & Buser incorporated observational flux corrections into these models for a range of stellar temperatures, but does not alter the $> 30K$ models of Kurucz. The STARBURST 99 code also uses the plane-parallel atmospheric Lejeune grid. For stars with strong winds it offers the choice of the Lejeune grid or the Schmutz, Leitherer & Gruenwald (1992) extended model atmospheres (hereafter known as the Schmutz atmospheres). The prescription for the switch between extended and plane-parallel atmospheres is the same as in Leitherer & Heckman (1995).

We ran models for both the “standard” mass loss rates and the “enhanced” mass loss rates described in Leitherer et al. (1999). We found that for the line diagnostic ratios used here, the mass loss prescriptions agree to within 0.03 dex.

Both codes follow the theoretical stellar tracks from the Zero Age Main Sequence (ZAMS) to their final stages. These stages include the asymptotic and post-asymptotic giant branch phases for intermediate-mass stars. The Padova tracks (Bressan et al. 1993) are used in PEGASE 2 and the Geneva tracks (Schaller et al. (1992)) are used in STARBURST99. The Padova tracks overshoot for masses $m \geq 1 M_{\odot}$ and use a higher ratio of the overshooting distance to the pressure scale height and down to lower masses than the Geneva tracks, which include overshooting only above $1.5 M_{\odot}$. Both tracks use the OPAL opacities; Iglesias, Rogers, & Wilson (1992) for the Padova Tracks and Rogers & Iglesias (1992) for the Geneva tracks. Both sets of tracks assume similar mixing lengths. Helium contents of 0.28 and 0.30 are used for the Padova and Geneva tracks respectively. The Padova tracks have a higher resolution in mass and time. Clear differences between these two sets of tracks (at solar metallicity) can be seen by comparing Figure (5) in Schaller et al. (1992) and Figure (7) in Bressan et al. (1993).

Assuming a standard initial mass function, the choices offered by the two spectral synthesis modeling codes allows sufficient flexibility to separately investigate, and to quantify, the effect that either the stellar atmospheres or the stellar evolutionary tracks have upon the theoretical starburst model line intensity ratios as a function of age. For example we can run the STARBURST99 code with either the Lejeune atmospheres or the Lejeune plus Schmutz atmospheres to investigate the effect of extended atmospheres, or we could compare the PEGASE 2 and STARBURST99 codes to quantify the effect of the differences between the Padova and the Geneva tracks and the effect of

the different stellar atmosphere models incorporated into these codes. We are confident that this comparison is valid, since in our earlier paper (Dopita et al. 2000), we compared the ionizing EUV spectra and H II region emission spectra predicted by the PEGASE and STARBURST99 codes for zero age clusters, and found these to be essentially identical.

In the modeling of the starburst emission spectra, we distinguish between a zero-age *instantaneous* star formation case, and *continuous* starburst models in which a balance between star birth and star death is set up for all stellar masses which contribute significantly to the EUV spectrum. The hydrogen-burning lifetime of massive stars is approximately $\tau = 4.5(M/40M_{\odot})^{-0.43}$ Myr, so in practice this condition is satisfied for any starburst which lasts longer than about 6 Myr. This gives a dynamical balance between star births and star deaths for all masses greater than about $20M_{\odot}$, and is also time enough for the Wolf Rayet stars to produce their full contribution to the EUV spectrum.

Figure (1) compares predicted solar metallicity EUV spectra produced by the PEGASE code which uses the Lejeune stellar atmospheres plus Clegg & Middlemass atmospheres for stars with high effective temperatures ($T > 50000\text{K}$), and the STARBURST99 codes which use either the Lejeune stellar atmospheres grid or the Lejeune atmospheres plus Schmutz extended model atmospheres. The PEGASE models used range from ages of 0 – 6 Myr, and the STARBURST99 models cover ages of 0 – 8 Myr. No further evolution in the shape of the EUV spectrum is seen after 6 and 8 Myr for the PEGASE and STARBURST99 models respectively.

After a few Myr of evolution, quite marked differences in the EUV spectrum develop. The comparison of Figure (1b) and Figure (1c) shows that the Schmutz extended atmospheres produce far more ionizing radiation at frequencies above the He II ionization limit than do the Lejeune atmospheres, but the differences are much less marked at lower energies. The differences between Figures (1a-c) are due to a combination of the different evolutionary tracks, and the stellar atmosphere models used. Figures (2) and (3) show the EUV spectra from PEGASE 2 and STARBURST99 for metallicities 0.2 and $2 \times$ solar. We can observe clear differences in the EUV spectra with increasing metallicity. In particular, the EUV spectrum becomes harder for lower age models. This is expected if high mass stars are responsible for the EUV field in this regime. At higher metallicities, the high mass stars make a larger contribution to the EUV radiation field at younger burst ages. The most likely cause of the difference between the EUV fields in Figures (1a-c) is to be found in the different stellar atmospheric models used for the high mass stars, especially for the Wolf-Rayet stars.

Since it was specifically constructed to model starbursts, the STARBURST99 code uses a more theoretically sophisticated approach to modeling the EUV spectrum. In the PEGASE 2 models, stars with effective temperatures greater than 50000 K (which includes Wolf-Rayet stars) are modeled by the Clegg & Middlemass planetary nebulae nuclei (PNN) atmospheres. These stars have much higher surface gravity than Wolf-Rayet stars, and so we would expect the atmospheric blanketing to be quite different. In STARBURST99 code, stars with strong stellar winds (which

includes Wolf-Rayet stars) are modeled by the Schmutz Wolf-Rayet atmospheres. These include H and He opacities, but do not include heavy element opacities.

The EUV spectrum emergent from a W-R model atmosphere depends critically on the fraction of ionizing photons which have been used up to maintain the ionization of the W-R wind region. This is determined by the size of the emission measure of the atmosphere; $\int n_e^2 dr$. This parameter is proportional to the the product $\left(\dot{M}/v_\infty\right)^2 R_*^{-3}$, where \dot{M} is the mass-loss rate, v_∞ the terminal velocity of the wind, and R_* is the photospheric radius of the star. This product is the Schmutz, Hamann, & Wessolowski (1989) density parameter. Models with the same density parameter display very similar emission line equivalent widths, but the total scaling in luminosity depends on R_*^2 . The density parameter can also be expressed in terms of a “transformed radius”, R_t :

$$R_t = R_* \left[\frac{v_\infty \dot{M}_{ref}}{v_{ref} \dot{M}} \right]^{2/3}$$

where v_{ref} is a (normalizing) reference velocity, and \dot{M}_{ref} is a (normalizing) reference mass-loss rate. Again, models with similar values of the transformed radius give similar spectra. Stars which use a greater fraction of their EUV photons in maintaining the photoionization of their extended atmospheres would show a lower-intensity, harder EUV spectrum below the He II ionization edge, and would be expected to exhibit more atmospheric blanketing by heavy elements.

4. Starburst Modeling

To model the starburst spectrum as a function of age of the exciting stars, metallicity and ionization parameter, we input the ionizing spectrum from the both continuous and instantaneous PEGASE and STARBURST99 models into the MAPPINGS III code. The photoionization modeling carried out with MAPPINGS III for this analysis is described in Dopita et al. (2000) and is described briefly here. We computed plane parallel, isobaric models with electron density of 350 cm^{-3} , which is the average electron density of the individual (frequently unresolved) H II regions within the 1 kpc slit aperture extracted for the starbursts in our sample. The electron density was found using the flux in the [S II] $\lambda 6716$ and [S II] $\lambda 6731$ forbidden lines from our spectra in conjunction with a 5 level model atom using MAPPINGS III. Electron densities for the galaxies in our sample can be found in Kewley et al. (2000a).

The ionization parameter q (cm s^{-1}) is defined on the inner boundary of the nebula, that is, the boundary nearest the exciting star. This dimensional ionization parameter can be readily transformed to the more commonly used dimensionless ionization parameter through the identity $\mathcal{U} \equiv q/c$.

Dust physics is treated explicitly through the absorption of the radiation field on grains, grain charging and photoelectric heating by the grains. We do not yet calculate the re-emission spectrum

of dust in the IR but this is currently being implemented. The dust model consists of silicate grains ($100\text{\AA} < a < 1000\text{\AA}$) and small amorphous organic grains ($10\text{\AA} < a < 100\text{\AA}$), with a size distribution following a Mathis, Rumpl & Nordsieck (1977) power-law and spherical geometry. The range of sizes is chosen so as to give depletion factors relative to solar similar to those observed by UV interstellar absorption measurements of stars seen through warm diffuse clouds in the local interstellar medium *eg* Jenkins (1987). The MAPPINGS III dust model also provides the observed absorption per hydrogen atom for solar metallicity (Bohlin, Savage & Drake 1978):

$$\frac{N(H)}{E_{B-V}} \sim 5.9 \times 10^{21} \text{ cm}^{-2} \text{ mag}^{-1}$$

Photoelectric yields are found using a more conservative yield curve of the same form as Draine & Sutin (1987). Photoelectric grain currents are found using Draine (1978) using the dust absorption data from Laor & Draine (1993). Collisions with electrons and protons are considered assuming the standard “sticking” coefficients, following Draine (1978) and Draine & Sutin (1987). More details of the dust physics in MAPPINGS III can be found in Dopita & Sutherland (2000).

The undepleted solar abundances are assumed to be those of Anders & Grevesse (1989); these abundances and the depletion factors adopted for each element in the starburst modeling are shown in Table 1. For non-solar metallicities we assume that both the dust model and the depletion factors are unchanged, since we have no way of estimating what they may be otherwise.

All elements except nitrogen and helium are taken to be primary nucleosynthesis elements. It is known that this assumption may be incorrect in systems where the time history of star formation in the galaxy is different, or where galactic winds are important. For example, the O/Fe ratio is different from its solar value in both the LMC and the SMC (Russell & Dopita 1992). Again, we are forced use the simplest assumptions possible in the absence of a more detailed understanding of the chemical evolution of starburst galaxies.

For helium, we assume a primary nucleosynthesis component in addition to the primordial value derived from Russell & Dopita (1992). This primary component is matched empirically to provide the observed abundances at SMC, LMC and solar abundances; Anders & Grevesse (1989), Russell & Dopita (1992). By number, the He/H ratio is:

$$\frac{\text{He}}{\text{H}} = 0.081 + 0.026(Z/Z_{\odot})$$

Nitrogen is assumed to be a secondary nucleosynthesis element above metallicities of 0.23 solar, but as a primary nucleosynthesis element at lower metallicities. This is an empirical fit to the observed behaviour of the N/O ratio in H II regions (van Zee, Haynes & Salzer, 1997). By number:

$$\begin{aligned} \log(\text{N}/\text{H}) &= -4.57 + \log(Z/Z_{\odot}) ; \log(Z/Z_{\odot}) \leq -0.63 \\ \log(\text{N}/\text{H}) &= -3.94 + 2 \log(Z/Z_{\odot}) ; \text{otherwise} \end{aligned}$$

The abundances and depletion factors for each element used can be found in Table 1.

The ionization parameter was varied from $q = 5 \times 10^6 \text{ cm s}^{-1}$ to $q = 3 \times 10^8 \text{ cm s}^{-1}$, and the metallicities varied from 0.01 to 3 solar for PEGASE and 0.05 to 2 solar for STARBURST99. The metallicity values used are restricted by the stellar tracks used by the population synthesis models.

4.1. Instantaneous Models

Figure (4) shows that, due to the absence of Wolf-Rayet stars, the use of similar zero-age Main Sequences, and the use of identical model atmospheres for massive stars, the shape of the EUV spectrum for both the PEGASE 2 and STARBURST99 models is almost identical for instantaneous burst models. As a consequence, they produce almost identical optical line ratios in the photoionization models. The results from these models are compared with the observational data set on the VO87 line ratio diagnostic diagrams in Figures (4), (5) and (6). Note that the major problem seen with these models is that many starburst galaxies are found in a region lying above and to the right of the “fold” in the ionization parameter : metallicity surface. This presents a problem, since these points lie in a “forbidden zone” of line ratio space which cannot be reached by any combination of metallicity or ionization parameter. The only way to make models which fall into this region of the the diagnostic diagrams is either to mix in another type of excitation *i.e.* shocks or a power-law ionizing radiation field or simply to use a harder EUV ionizing spectrum, particularly in the 1-4 Rydberg region.

In any event, we should not be too surprised that the instantaneous models do not provide a very good fit to the observed starbursts, since many of these objects are seen in merging pairs of galaxies, and in this case we would theoretically expect star formation to continue over a galactic dynamical timescale. Thus massive clusters associated with individual (usually unresolved) H II regions should have a wide variety of ages. Direct evidence for continuous star formation, or older H II regions, is seen in many of our starburst spectra. These show either a low equivalent width in H β (which often indicates dilution by an older stellar population) or clear evidence of H β absorption in the stellar continuum. Both of these indicate that star formation has continued over at least several Myr (González Delgado & Leitherer 1999).

In Dopita et al. (2000), we showed that the line ratio usually used for measuring the ionization parameter; [O III] $\lambda 5007$ / [O II] $\lambda \lambda 3726,9$, is indeed a good diagnostic and that the [N II] $\lambda 6584$ / [O II] $\lambda \lambda 3726,9$ ratio gives the best diagnostic of abundance, as it is monotonic between 0.1 and over 3.0 times solar metallicity. The wavelength range of our spectra was not sufficient for us to observe [O II], however we present the grids of the instantaneous models for the [N II] $\lambda \lambda 6548,84$ / [O II] $\lambda \lambda 3726,9$ *vs.* [O III] $\lambda 5007$ / H β diagram and the [N II] $\lambda \lambda 6548,84$ / [O II] $\lambda \lambda 3726,9$ *vs.* [O III] $\lambda 5007$ / [O II] $\lambda \lambda 3726,9$ in Figures (7) and (8) for the use of the astronomical community.

4.2. Continuous Models

As we have seen, when star formation continues over several Myr, the ionizing spectrum evolves until a dynamic balance between stellar births and stellar deaths has been set up for all initial stellar masses which are important in producing EUV photons. As Figure (1) shows, this occurs after 6 and 8 Myr for the PEGASE and STARBURST99 models respectively, and so these cluster ages were assumed for the continuous star formation models presented in this section.

The results for the continuous models shown on the VO87 line ratio diagnostic diagrams are presented in Figures (9-11) for the PEGASE 2 models with (a) the Lejeune plus Clegg & Middlemass PNN model atmospheres, (b) the STARBURST99 models with the Lejeune plus Schmutz model atmospheres and (c) the STARBURST99 models with the Lejeune atmospheres respectively.

Let us first consider the two sets of STARBURST99 models. The differences seen here simply reflect the differences in the stellar atmospheric models. The Lejeune plus Schmutz model atmospheres show little change in spectral slope between 1 and 3 Ryd as a function of cluster age. It is therefore not surprising that these continuous star formation models give very similar results to the zero age instantaneous models of Figures (4 - 8). In these continuous star formation models the W-R stars provide a radiation field of appreciable strength above the He II ionization limit (eg. 4-8 Ryd in Figures 1-3). In this case, we might expect to detect He II lines in the optical spectrum. The detection of a nebular He II $\lambda 4686$ line would provide an important observational diagnostic in support of the Schmutz extended atmospheric modeling and is discussed in the following section.

These models with Schmutz extended atmospheres have exactly the same difficulty in explaining the position of the observed points as do the instantaneous models, in that the model grid fails to overlap about half of the observed points, indicating the need for a harder ionizing spectrum than these tracks and atmospheres provide.

The second of the STARBURST99 grids, for continuous starbursts using the Geneva tracks along with the Lejeune atmospheres provides an even softer radiation field in the 1 – 4 Ryd energy range. In this case, the theoretical grid falls below and to the left of the majority of the observed points on all three of the VO87 plots. This combination of tracks and atmospheres is therefore excluded with a good degree of certainty.

Finally, consider the PEGASE 2 models, which use the Padova tracks with the Lejeune plus Clegg & Middlemass PNN extended atmospheres. These models are characterised by the hardest radiation field in the 1 - 4 Ryd region, and are the only ones that show the spectrum becoming harder as the W-R stars turn on. This is a direct consequence of the Clegg & Middlemass PNN atmosphere models used for stars with effective temperatures greater than 50000 K. These are the only set of models which encompass nearly all of the observed starbursts on all three of the VO87 line diagnostic plots. Furthermore, individual objects fall into similar regions of the theoretical grid in all three diagnostic plots, indicating that there is some degree of consistency achieved here. In essence, the ionization parameter appears to be limited to the range $6 \times 10^6 \gtrsim q \gtrsim 6 \times 10^7$ and

the metallicity range seems to cover most of the range; from about 0.2 solar up to nearly 3 times solar. However, the low-metallicity objects appear to be rather rare in our sample, and most of the starbursts are consistent with a metallicity 1 - 3 times solar.

We present the grids of the continuous models for the [N II] $\lambda\lambda 6548,84$ / [O II] $\lambda\lambda 3726,9$ *vs.* [O III] $\lambda 5007$ / $H\beta$ diagram and the [N II] $\lambda\lambda 6548,84$ / [O II] $\lambda\lambda 3726,9$ *vs.* [O III] $\lambda 5007$ / [O II] $\lambda\lambda 3726,9$ in Figures (12) and (12) for the use of the astronomical community.

4.3. Shock Excitation from Supernovae

The starburst models presented here are based on pure photoionization models, and therefore do not incorporate the effect of mechanical luminosity from supernovae shocks. The primary effect of the release of mechanical energy through shocks is to move the theoretical grids upwards, and lightly to the right on the VO87 line ratio diagnostic plots. The size of this effect depends on the relative importance of the shock and photoionization luminosity.

The input mechanical energy luminosity \dot{E}_{mech} produced by supernova events and winds is converted into optical line emission through radiative shocks. The importance of this line emission relative to that produced by photoionization depends on fraction of this energy, ϵ , which has been converted to $H\beta$ flux compared to the $H\beta$ flux produced by recombinations in the photoionized plasma:

$$\frac{L_{H\beta}(\text{shock})}{L_{H\beta}(\text{photo})} = \frac{\epsilon \dot{E}_{\text{mech}}}{\alpha_{\text{eff}} h \nu_{H\beta} S_*} \quad (1)$$

where α_{eff} is the effective recombination coefficient of hydrogen, and S_* is the number of ionizing photons being produced by the hot stars in the cluster.

In the case of a supernova remnant, the shock becomes radiative, and the Sedov-Taylor (adiabatic) expansion phase is terminated when its cooling timescale, τ_{cool} , becomes shorter than the dynamical expansion timescale of the shell, τ_{exp} . From standard Sedov-Taylor theory, $\tau_{\text{exp}} = R/v_s = 5t/2$ where R is the radius of the supernova remnant, v_s is the shock wave velocity, and t is the time since the supernova explosion. The radiative shock-wave theory of Dopita & Sutherland (1996) shows that the cooling timescale, in years, can be expressed as:

$$\tau_{\text{cool}} \sim 200 \frac{v_{100}^{4.4}}{Zn} \quad (2)$$

where v_{100} is the shock velocity in units of 100 km s⁻¹, Z is the metallicity of the plasma relative to solar, and n is the pre-shock density. We therefore find that, with $n \sim 350$ cm⁻³, a supernova remnant typically become radiative at a radius of 1 pc, when the shock velocity is 600

km s⁻¹. At this point, the supernova remnant is ~ 600 years old, and its expansion timescale is ~ 1500 yr.

We therefore used a shock model with a velocity of 600 km s⁻¹ in a spherical nebula of solar metallicity and $n \sim 350$ cm⁻³ to calculate the possible contribution by supernova remnants to our photoionization models. We assumed a total mechanical luminosity in SNR of 6×10^{41} erg/s/M_⊙/yr (Leitherer et al. 1999). We calculated a star formation rate of ~ 3.4 M_⊙/yr from the average L_{IR} for the starbursts in our sample, following the prescription given in Kennicutt (1998) (note that L_{IR} is defined as L_{FIR} in Kennicutt (1998)). Assuming the IR luminosity is distributed evenly throughout the galaxy and a minimum size of 7 kpc, the SFR reduces to ~ 0.07 M_⊙/yr in the observed aperture. We note that this is still higher than that found using the H α luminosity of our template starburst (within the 1 kpc aperture) of ~ 0.04 M_⊙/yr. This is to be expected as dust absorption will reduce the H α derived SFR compared with that derived using the FIR luminosity. We computed a 600 km/s shock model and a spherical ionized precursor with a shocked spherical radius of 1 pc. This model had a mechanical luminosity of 3.6×10^{39} erg/s. As we expect the total mechanical luminosity to be $\sim 4 \times 10^{40}$ erg/s, we expect to obtain on average 11.2 SNR within our 1 kpc aperture at any one time. The luminosity produced in the shock and precursor are given in Table (2).

From this SNR model, the contribution to H β emission in the starbursts due to SNRs would be about 16-20%. The contribution to the H β flux from starbursts is determined more or less directly by the star formation history and the IMF. The contribution to H β from SNRs is determined by the velocity and the total area covered by the SNR shocks, which in turn depend on the number of SNRs (determined by the SFR and IMF) and weakly on the density. At low densities, SNRs are larger and have lower velocities than at higher densities, and have similar overall luminosities in H β .

The [O III] emission from the starbursts, on the other hand, is not a function of the SFR, rather it is a measure of the ionization parameter q of the radiation field within the starburst which is a function of the density and mass distribution (ie filaments vs uniform) of the gas. Thus the [O III] in the starburst models varies from bright to negligible levels compared to H β . The [O III] mission from the SNRs is constrained by the chosen model geometry and is therefore determined by the SFR and the average density, not by the global ionization parameter. The ionization parameter for each SNR is determined internally by the SNR model without reference to the global starburst value.

The observed total $\log([O III]/H\beta)$ ratio is the sum of the starburst and SNR contributions;

$$\log([OIII]/H\beta) = \log([OIII]_{\text{starb}} + [OIII]_{\text{SNR}}) - \log(H\beta_{\text{starb}} + H\beta_{\text{SNR}}). \quad (3)$$

Thus, in the limit of $[OIII]_{\text{starb}} = 0$ due to low global q in the starbursts, the observed $\log([O III]/H\beta)$ ratio will reach a lower limit of

$$\log([\text{OIII}]_{\text{SNR}}) - \log(\text{H}\beta_{\text{starb}} + \text{H}\beta_{\text{SNR}}) \geq 0.0 \quad (4)$$

with a density of 350 cm^{-3} and the SFR used here ($\sim 0.07 \text{ M}_{\odot}/\text{yr}$ in the observed aperture of 1 square kpc).

This lower limit is not observed, and the actual lower limit is $\log([\text{OIII}]/\text{H}\beta) \approx -1.0$, a factor of 10 less than the SNR model limit. Clearly the strong $[\text{OIII}]_{\text{SNR}}$ contribution modeled here is not compatible with the observations. This incompatibility may be due to either the number of SNR we derived, or that the average density in the SNR environment is less than 350 cm^{-3} . We conclude that the SNR contribution to the $\log([\text{O III}]/\text{H}\beta)$ ratio is $\ll 20\%$ and is probably a factor of 10 less ($\sim 2\%$), and can be neglected for the starburst models derived here. We are currently investigating this SNR contribution to starbursts further by considering a range of densities and lower shock velocities to determine the level at which the SNRs model is compatible with the observations. We expect to find that velocities in the 200-300 km/s range will be more compatible with observations, resulting in a small $[\text{OIII}]_{\text{SNR}}$ contribution, negligible in all but the starbursts with the lowest ionization parameter.

5. Wolf-Rayet Emission in Starburst Galaxies

Wolf-Rayet features were first found in the dwarf emission galaxy He2-10 (Allen, Wright, & Goss 1976). As more such features were discovered in galaxies, Osterbrock & Cohen (1982) defined Wolf-Rayet (W-R) galaxies as those galaxies which contain broad stellar emission lines in their spectra and therefore contain large numbers of W-R stars. The large numbers of W-R stars are thought to be a result of present or very recent star formation. Kunth & Joubert (1985) searched for W-R emission in a sample of blue emission-line galaxies. They found a positive detection in one galaxy and suspected in 14 others and suggested that W-R stars are preferentially detected in low redshift galaxies. The first catalogue of W-R galaxies was presented by Conti (1991), showing that W-R galaxies can be easily distinguished by their broad $\lambda 4686$ [He II] emission feature, or in some cases a broad line at 4640\AA due to N III. High resolution long-slit observations of a sample of Wolf-Rayet galaxies were carried out recently by Guseva, Izotov, & Thuan (2000). Nearly all the galaxies in their sample show broad W-R emission consisting of an unresolved blend of N III $\lambda 4640$, C III $\lambda 4650$, [Fe III] $\lambda 4658$, and He II $\lambda 4686$ emission lines. They also found weaker W-R emission lines N III $\lambda 4512$ and Si III $\lambda 4565$ in some galaxies.

The signal-to-noise ratios of our spectra are not sufficient in individual galaxies to detect these signatures of W-R emission. We have therefore constructed a template “average” warm infrared starburst spectrum from the 56 starburst galaxies in our sample which have SNRs at $\text{H}\beta$ of 60 or greater and for which the zero-redshift blue wavelength cut-off is lower than $\lambda 4620$. We note that this average spectrum is not representative of our sample of warm infrared starbursts because selecting for high SNR galaxies may bias the average spectrum towards young and hence more

luminous starbursts. However, it is useful simply to assist in the search for W-R features. The average spectrum is shown in Figure (14) and in detail in Figure (15). The positions of the expected W-R features are marked on Figure (15).

The mean age of the average warm infrared starburst can be estimated from the $H\beta$ absorption equivalent width, bearing in mind that dust absorption may also contribute to the absorption line profile and has not been taken into account. The $H\beta$ absorption equivalent width was found by simultaneously fitting the $H\beta$ absorption and emission lines with gaussians in the IRAF task *ngaussfits*. We find that the $H\beta$ absorption equivalent width is $\sim 3.6 \text{ \AA}$ which corresponds to an upper limit age of $\sim 7 \text{ Myr}$ for a continuous star formation model at solar metallicity (González Delgado & Leitherer 1999). However, this is probably an underestimate, since the $H\beta$ absorption equivalent width will be reduced by any underlying old star population. Nonetheless, there is likely to be a selection effect towards more youthful starbursts, in that the bright starbursts tend to be both younger and intrinsically more luminous.

In the “average” spectrum of Figure (15), there appears to be marginal detections of [Fe III] $\lambda 4658$, and He II $\lambda 4686$ at the 2σ level. These lines do not appear broad, however this may simply be an effect of the low SNR for these lines.

The He II $\lambda 4686$ emission in the majority of our galaxies provides an important constraint on the Schmutz extended atmospheric modeling. The $\log(\text{He II } \lambda 4686/H\beta)$ ratio for our template starburst galaxy is ~ -1.6 . Both the MAPPINGS III models with PEGASE and STARBURST99 (Lejeune atmospheres) stellar ionizing continua produce $\log(\text{He II } \lambda 4686/H\beta)$ around -6 , while the MAPPINGS III models with STARBURST99 (Lejeune + Schmutz atmospheres) stellar ionizing continuum produces $\log(\text{He II } \lambda 4686/H\beta)$ around -1.7 , consistent with that observed with our template starburst galaxy. We note again that our template starburst galaxy has been composed of the starbursts in our sample with the highest SNRs, and so may be biased towards the most luminous and therefore the youngest starbursts in our sample. This He II $\lambda 4686/H\beta$ ratio for our template starburst may therefore be biased towards those with more W-R stars than the average starburst galaxy in our sample. Clearly we require a hard EUV field in the 1-4 Ryd regime to model our starburst galaxies on the optical diagnostic diagrams such as that provided with the PEGASE 2 model. However, as we would expect the Schmutz extended atmospheric modeling to be more appropriate to the modeling of our starburst galaxies, we believe that the inclusion of continuum metal opacity (or continuum metal blanketing) in the stellar population synthesis models using the Schmutz extended atmospheres is a possible solution.

6. Continuum Metal Opacity

For many years, optical depth estimates in the ISM were found using the hydrogen 21cm line and the assumption of a uniform gas density. As a result of the low optical depths obtained, it was thought that the ISM should be opaque to radiation in the EUV (Aller 1959). The discovery that the

ISM is inhomogeneous overturned this conclusion and Cruddace et al. (1974) established an estimate of the effective absorption cross-section of the ISM at EUV wavelengths using determinations of cross-sections and abundances. Cruddace et al. (1974) showed that some EUV radiation should be able to be observed over considerable distances. More recent determinations of cross-sections and abundances have been used by Rumph, Bowyer, & Vennes (1994) to provide a new estimate of the effective absorption cross-section of the ISM at EUV wavelengths.

The relative difficulty in obtaining EUV spectra to compare with theoretical estimates of opacity in the EUV continuum described above has decreased significantly over the last decade with the aid of EUV telescopes such as EUVE (Extreme Ultraviolet Explorer), ROSAT Wide Field Camera, ALEXIS (Array of Low Energy X-ray Imaging Sensors), FUSE (Far Ultraviolet Spectroscopic Explorer), and the Extreme-Ultraviolet Imaging Telescope (EIT). These telescopes have allowed observations of many stellar objects which have greatly advanced the modeling of stellar atmospheres (Cassinelli 1995, eg.) and have allowed the EUV study of some Seyfert galaxies (eg. Hwang & Bowyer (1997)). However the EUV spectrum in starburst galaxies continues to remain unseen as a result of the weakness of the EUV continuum in starburst galaxies due to absorption. It is therefore necessary to rely on theoretical predictions of the EUV spectrum from stellar population synthesis codes.

Although the EUV spectrum must be estimated using theoretical modeling, the reprocessing of the EUV spectrum into optical emission lines allows limits to be placed on the shape of the EUV spectrum in starburst galaxies. As concluded in previous sections, we require a harder EUV field between the 1-4 Ryd regime than is provided by the stellar population synthesis models with Schmutz extended atmospheres. Currently, only continuous opacities due to helium are included in the models, as continuous metal opacities are relatively unimportant for many studies. We believe that the inclusion of continuum metal opacities in these models would provide a suitable shape in the EUV, enabling the models to reproduce the starburst sequence on the standard optical diagnostic diagrams.

Continuum metal opacities, as with hydrogen and helium opacities, are a result of bound-free transitions, ie photoionization of the metals. Continuum metal opacity would allow some fraction of the radiation with energies greater than 4 Ryd to be absorbed and re-emitted less than 4 Ryd. The fraction of radiation absorbed by metals depends on their individual absorption cross-sections and abundances. The resulting EUV continuum would have a softer continuum above the He II ionization limit, as a result of carbon opacities. The spectrum would also have a harder but fainter EUV field between the 1-4 Ryd regime, as required by the position of our starburst galaxies on the optical diagnostic diagrams. Note that if this were the case, we might expect that the models with Schmutz extended atmospheres would produce too much flux in the He II $\lambda 4686$ line compared with our observations, contrary to our findings. We conclude that while continuum metal blanketing may be a possible solution to the discrepancy seen between our observations and the models using Schmutz extended atmospheres, it may not be the only solution.

7. Extreme Starburst Classification Line

In order to place a theoretical upper limit for starburst models on the optical diagnostic diagrams, we used the PEGASE 2.0 grids, since these provide the hardest EUV spectrum, and therefore give a theoretical grid which is placed both highest and furthest to the right on the VO87 line ratio diagnostic diagrams.

We have shown that, with a realistic range of metallicities ($Z = 0.1 - 3.0$) and ionization parameter q (cm/s) in the range $5 \times 10^6 \leq q \leq 3 \times 10^8$ (or $-3.5 \leq \log \mathcal{U} \leq -2.0$), continuous starburst models produced by any modeling procedure always fall below and to the left of an empirical limit on the $[\text{N II}]/\text{H}\alpha$ vs. $[\text{O III}]/\text{H}\beta$, $[\text{S II}]/\text{H}\alpha$ vs. $[\text{O III}]/\text{H}\beta$ and $[\text{O I}]/\text{H}\alpha$ vs. $[\text{O III}]/\text{H}\beta$ diagrams. This is due to the two-parameter grid of the ionization parameter and metallicity folding back upon itself. Therefore, no combination of these parameters can generate a theoretical point above this fold. The lines dividing the theoretical starburst region from objects of other types of excitation are shown in Figure (16). These can be parametrized by the following simple fitting formulae, which have the shape of rectangular hyperbolae;

$$\log \left(\frac{[\text{OIII}] \lambda 5007}{\text{H}\beta} \right) = \frac{0.61}{\log([\text{NII}]/\text{H}\alpha) - 0.47} + 1.19 \quad (5)$$

$$\log \left(\frac{[\text{OIII}] \lambda 5007}{\text{H}\beta} \right) = \frac{0.72}{\log([\text{SII}] \lambda \lambda 6717, 31/\text{H}\alpha) - 0.32} + 1.30 \quad (6)$$

$$\log \left(\frac{[\text{OIII}] \lambda 5007}{\text{H}\beta} \right) = \frac{0.73}{\log([\text{OI}] \lambda 6300/\text{H}\alpha) + 0.59} + 1.33 \quad (7)$$

The shape and position of this maximum starburst line has not been previously established from theoretical models, since the shape of the ionizing spectrum of the cluster has not been known to sufficient accuracy. VO87 have attempted to establish both the position and the shape of this boundary in a semi-empirical way, using both observational data from the literature and a combination of models available to them at that time.

The theoretical boundaries for starbursts defined by equations (1)-(3) provide us for the first time with a theoretical (as opposed to a semi-empirical boundary) for the region occupied by starbursts in these diagnostic plots. In view of the potential for errors in the modeling which may flow from errors in the assumptions made in the chemical abundances, chemical depletion factors, the slope of the initial mass function, and the evolutionary tracks and the stellar atmosphere models used, we have indicated a “best guess” estimate of these errors as dashed lines in Figure (16).

These theoretical upper limits for starburst galaxies have been used in Kewley et al. (2000a) to classify the galaxies in our sample along with an ‘extreme’ mixing line produced using our shock modeling to classify galaxies into starburst, LINER and AGN types. The strength of our theoretical starburst classification line can be seen by observing the number of galaxies which have ‘ambiguous’

classifications. These galaxies are those which fall within the starburst region of one or two of the diagnostic diagram(s) and the AGN region of the remaining diagram(s). We found that only 6% of our sample have ambiguous classifications using our theoretical extreme starburst line, compared with 16% ambiguous classifications using the standard VO87 classification lines. These results indicate that our theoretical starburst line is a reliable tool for optically classifying galaxies into starburst and AGN types, and is more consistent from diagram to diagram than the conventional VO87 method.

8. Conclusions

We have presented a comparison between the stellar population synthesis models PEGASE 2 and STARBURST99 using a large sample of 157 warm infrared starburst galaxies. The main differences between the two synthesis models are the stellar tracks and stellar atmosphere prescriptions. PEGASE and STARBURST99 were used to generate the spectral energy distribution (SED) of the young star clusters. MAPPINGS III was used to compute photoionization models which include a self-consistent treatment of dust physics and chemical depletion. The standard optical diagnostic diagrams are indicators of the hardness of the EUV radiation field in the starburst galaxies. These diagnostic diagrams are most sensitive to the spectral index of the ionizing radiation field in the 1-4 Rydberg region. We find that warm infrared starburst galaxies contain a relatively hard EUV field in this region. The PEGASE ionizing stellar continuum is harder in the 1-4 Ryd range than that of STARBURST99, most likely due to the different stellar atmospheres used for Wolf-Rayet stars.

We have constructed an average spectrum of the high SNR warm infrared starbursts in our sample in order to look for Wolf-Rayet signatures. We find detections of C IV $\lambda 4658$, and He II $\lambda 4686$ at the 2σ level, indicating W-R activity, and constraining the Schmutz extended atmospheric modeling. We require a hard EUV field in the 1-4 Ryd regime to model our starburst galaxies on the optical diagnostic diagrams such as that provided with the PEGASE 2 model. However, as we would expect the Schmutz extended atmospheric modeling to be more appropriate to the modeling of our starburst galaxies, we believe that one solution would be to include continuum metal blanketing in the stellar population synthesis models using the Schmutz extended atmospheres. Continuum metal blanketing would allow much of the radiation with energies greater than 4 Ryd to be absorbed and re-emitted at energies less than 4 Ryd. The resulting EUV continuum would have a softer continuum above the He II ionization limit and a harder EUV field between the 1-4 Ryd regime, as required by the position of our starburst galaxies on the optical diagnostic diagrams. SNRs could also contribute to the hardness of the EUV field, although our models and observations suggest that this is likely to be $\ll 20\%$, insufficient to cause the discrepancy between our starburst galaxies and the models using Schmutz extended atmospheres.

We use the starburst grids produced with the PEGASE EUV ionizing radiation field and our MAPPINGS III models to parametrize an extreme starburst line which is useful in classifying

galaxies into starburst or AGN types. In a previous paper (Kewley et al. 2000a), we showed that this theoretical classification scheme produces reliable classifications with less ambiguity than the classical Veilleux & Osterbrock (1987) empirical method.

9. Acknowledgements

We thank Claus Leitherer and Brigitte Rocca-Volmerange for helpful discussions and for the use of STARBURST99 and PEGASE 2. We thank the referee for his constructive comments which helped this to be a better paper. We also thank the staff at Siding Springs Observatories for their assistance during our spectroscopy observations. L. Kewley gratefully acknowledges support from the Australian Academy of Science Young Researcher Scheme and the French Service Culturel & Scientifique.

REFERENCES

- Allen, D. A., Wright, A. E. & Goss 1976, MNRAS, 177, 91
- Aller, L. H., 1959, PASP, 71, 324
- Anders, E. & Grevesse, N. 1989, Geochim. & Cosmochim. Acta 53, 197
- Armus, L., Heckman, T. M., & Miley, G. K. 1989, ApJ, 347,727
- Armus, L., Heckman, T. M., & Miley, G. K. 1990, ApJ, 364, 471
- Baldwin, J. A., Phillips, M. M., & Terlevich, R. 1981, PASP, 93, 5
- Bessell, M. S., Brett, J. M., Scholz, M., & Wood, P. R. 1989, A&AS, 77, 1
- Bessell, M. S., Brett, J. M., Scholz, M., & Wood, P. R. 1991, A&AS, 89, 335
- Bohlin, R.C., Savage, B.D., & Drake, J.F. 1978, ApJ, 224, 132
- Bressan, A., Fagotto, F., Bertelli, G., & Chiosi, C. 1993, A&AS, 100, 647
- Cassinelli, J. P., Cohen, D. H., Macfarlane, J. J., Drew, J. E., Lynas-Gray, A. E., Hoare, M. G., Vallergera, J. V., Welsh, B. Y., Vedder, P. W. Hubeny, I., & Lanz, T. 1995, ApJ, 438, 932
- Clegg, R.E.S. & Middlemass, D. 1987, MNRAS, 228, 759
- Conti, P. S. 1991, ApJ, 377, 115
- Cruddace, R., Paresce, F., Bowyer, S., & Lampton, M. 1974, ApJ, 187, 497
- Dopita, M. A., Kewley, L. J., Heisler, C. A., & Sutherland, R. S. 2000, ApJ, in press (October 10)

- Dopita, M. A. & Sutherland, R. S. 2000b ApJ, 539, 742
- Dopita, M. A., & Sutherland, R. 1996, ApJS, 102, 161
- Draine, B. T. 1978, ApJS, 36, 595
- Draine, B. T. & Sutin, B. 1987, ApJ, 320, 803
- Ferland, G. J., Korista, K. T., Verner, D. A., Ferguson, J. W., Kingdon, J. B., & Verner, E. M. 1998, PASP, 110, 761
- Fioc, M., & Rocca-Volmerange, B. 1997, A&A, 326, 950
- Fluks, M. A., et al., 1994, A&AS, 105, 311
- Genzel, R. et al. 1998, ApJ, 498, 579
- González Delgado, R. M. & Leitherer, C. 1999, ApJS, 125, 479
- Guseva, N. G., Izotov, Y. I., & Thuan, T. X. 2000, ApJ, 531, 776
- Hwang, C.-Y., & Bowyer, S. 1997, ApJ, 475, 552
- Iglesias, C. A., Rogers, F. J., & Wilson, B. G. 1992, ApJ, 397, 717
- Jenkins, E.B. 1987, in “Interstellar Processes”, eds. D.J. Hollenbach & H.A. Thronson, Jr. (Dordrecht:Reidel), Astrophys. Space Sci. Library, 134, 533
- Kennicutt, R. C. Jr. 1998, ARA&A, 36, 189
- Kewley, L. J., Heisler, C. A., Dopita, M. A., & Lumsden, S. 2000, ApJS, in press
- Kewley, L. J., Heisler, C. A., Dopita, M. A., Sutherland, R. S., Norris, R. P., Reynolds, J., & Lumsden, S. 2000, ApJ, 530, 704
- Kunth, D. & Joubert, M. 1985, A&A, 142, 411
- Kurucz, R.L. 1992, in IAU Symp. 149, The Stellar Populations of Galaxies, ed. B. Barbuy & A. Renzini (Dordrecht:Kluwer), 225
- Laor, A. & Draine, B. T. 1993, ApJ, 402, 441
- Leitherer, C. & Heckman, T.M. 1995, ApJS, 96, 9
- Leitherer, C., Schaerer, D., Goldader, J. D., Delgado, R. M. González, R. C., Kune, D. F., de Mello, Duília F., Devost, D., & Heckman, T. M. 1999, ApJS, 123, 3
- Lejeune, Th., Cuisinier, F. & Buser, R. 1997, A&AS, 125, 229

- Lutz, D., Genzel, R., Sternberg, A., Netzer, H., Kunze, D., Rigopoulou, D., Sturm, E., Egami, E., Feuchtgruber, H., Moorwood, A. F. M., & de Graauw, T. 1996, *â*, 315, 137
- Lutz, D., Spoon, H. W. W., Rigopoulou, D., Moorwood, A. F. M., & Genzel, R. 1998, *ApJ*, 505, 103
- Mathis, J.S., Rumpl, W. & Nordsieck, K.H. 1977, *ApJ*, 217, 425
- Miley, G. K., Neugebauer, G., & Soifer, B. T. 1985, *ApJ*, 293, 11
- Osterbrock, D. E. & Cohen, R. D. 1982, *ApJ*, 261, 64
- Osterbrock, D. E., & de Robertis, M. M. 1985, *PASP*, 97, 1129
- Rieke, G.H., & Low, F.J. 1972, *ApJ*, 176, 95
- Rogers, F. J. & Iglesias, C. A. 1992, *ApJS*, 79, 507
- Rumph, T., Bowyer, & Vennes, S. 1994, *AJ*, 107, 2108
- Russell, S. C. & Dopita, M.A. 1992, *ApJ*, 384, 508
- Schaller, G., Schaerer, D., Meynet, G., & Maeder, A. 1992, *A&AS*, 96, 269
- Schmutz, W., Hamann, W.-R., & Wessolowski, U. 1989, *A&A*, 210, 236
- Schmutz, W., Leitherer, C. & Gruenwald, R.B. 1992, *PASP*, 104, 1164
- Strauss, M. A., Huchra, J. P., Davis, M., Yahil, A., Fisher, K. B., & Tonry, J. 1992, *ApJS*, 83, 29
- Sutherland, R.S. & Dopita, M.A. 1993, *ApJS*, 88, 253
- van Zee, L., Haynes, M. P., & Salzer, J. J., 1997, *AJ*, 114, 2497
- Veilleux, S., Kim, D.-C., Sanders, D.B. 1999, *ApJ*, 522, 113
- Veilleux, S., Kim, D.-C., Sanders, D.B., Mazzarella, J.M., & Soifer, B.T. 1995, *ApJS*, 98, 171
- Veilleux, S., & Osterbrock, D.E. 1987, *ApJS*, 63, 295

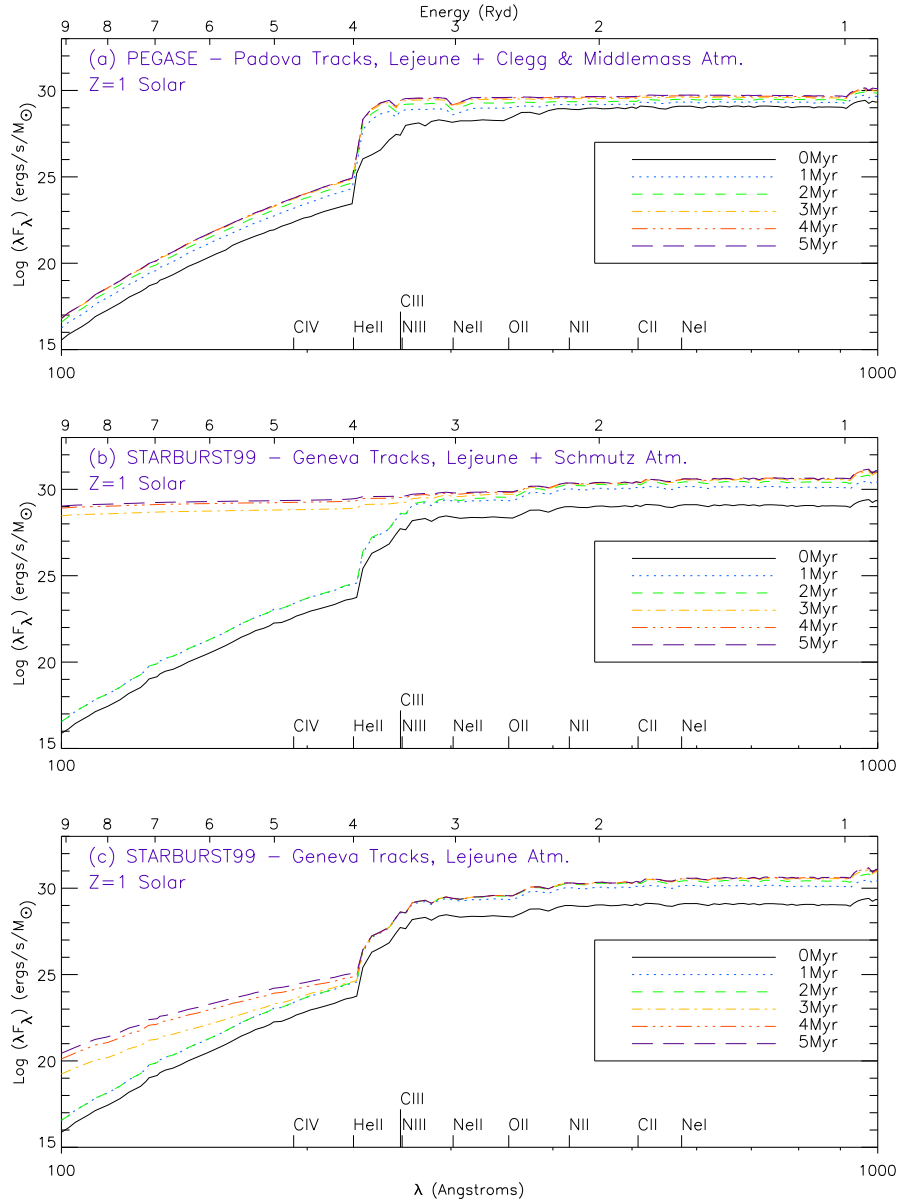


Fig. 1.— The ionizing spectral energy distribution (normalised to the flux at the Lyman limit) as a function of age of the starburst for (a) the PEGASE models, (b) and the Lejeune plus Schmutz atmospheres and (c) the STARBURST99 models for Lejeune atmospheres. Ionization edges are shown for some elements. Note the rapid initial evolution as the Wolf-Rayet stars evolve, and the convergence toward an asymptotic solution when a stochastic balance between star births and star deaths is achieved for all masses which contribute to the EUV continuum. All models produce very similar results at zero age, but differ markedly at later times, mainly reflecting differences between the extended stellar atmosphere models used (Clegg & Middlemass (1987) for PEGASE and Schmutz, Leitherer & Gruenwald (1992) for STARBURST99).

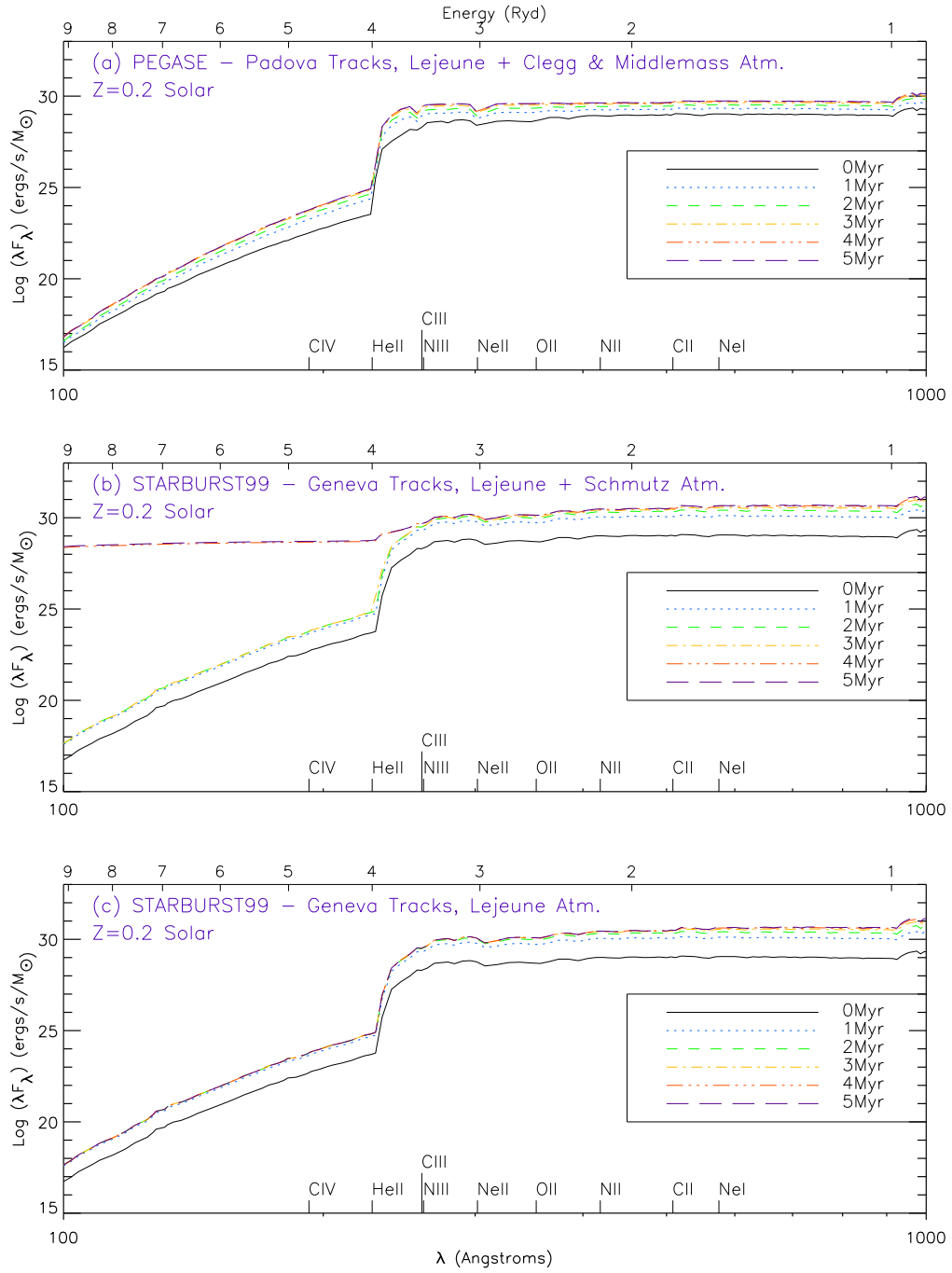


Fig. 2.— As in Figure 1, except $Z=0.2 \times$ solar metallicity.

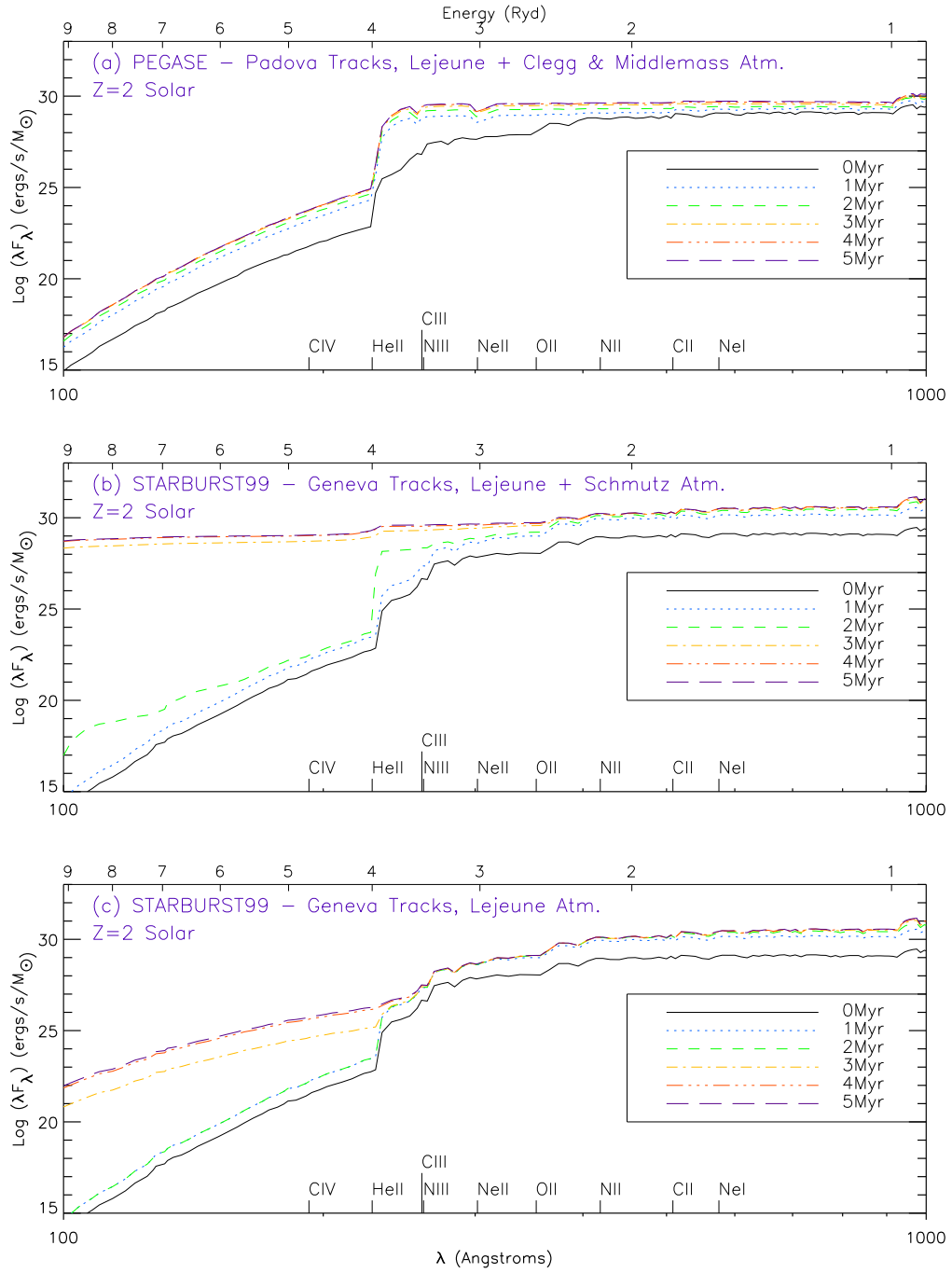


Fig. 3.— As in Figure 1, except $Z=2 \times$ solar metallicity.

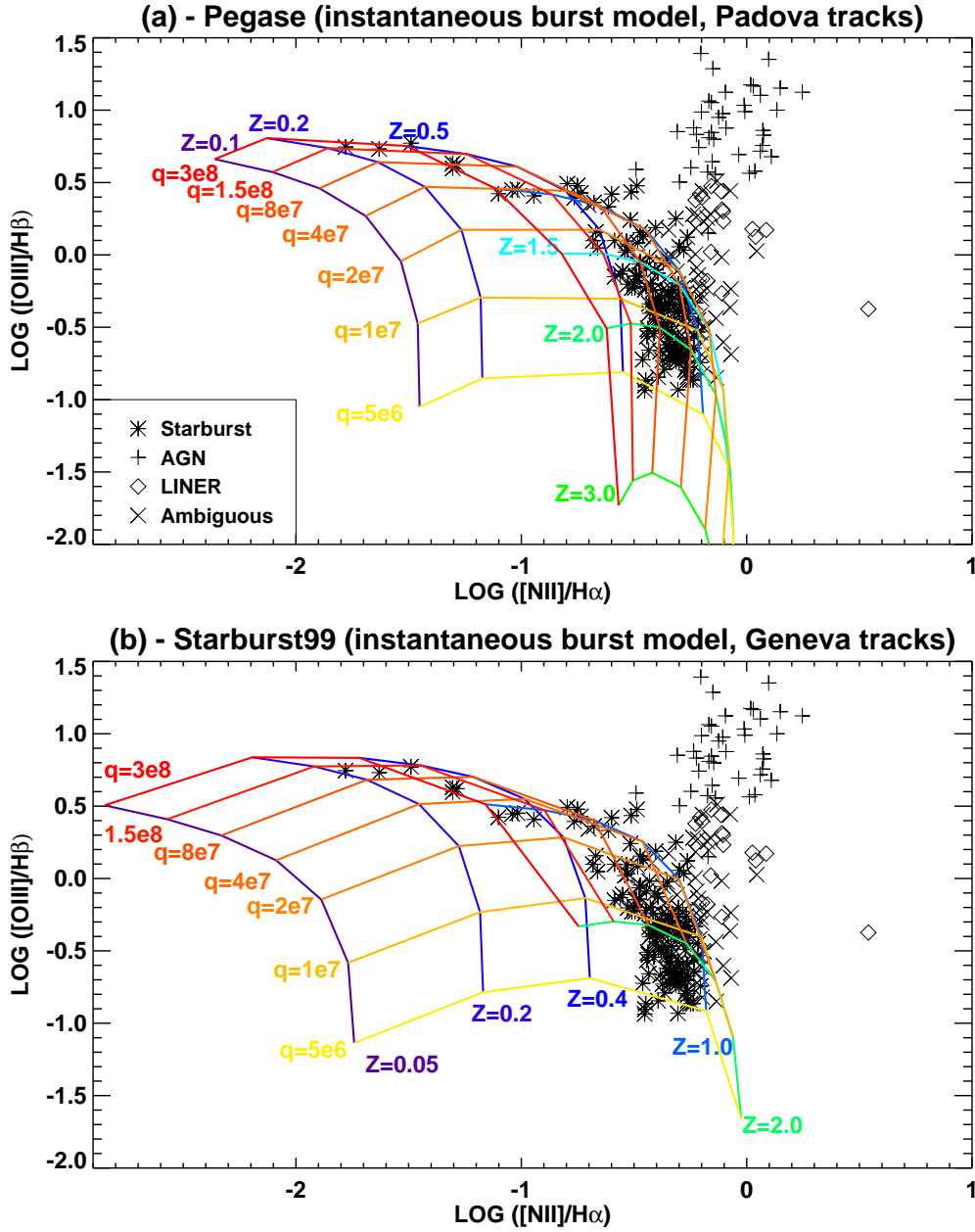


Fig. 4.— The Veilleux & Osterbrock (1987) diagnostic diagram $\log [\text{NII}]/\text{H}\alpha$ \log vs $\log [\text{OIII}]/\text{H}\beta$ for (a) the instantaneous zero-age starburst models based on the PEGASE spectral energy distribution, (b) instantaneous zero-age starburst models based on the STARBURST99 spectral energy distribution with Lejeune plus Schmutz atmospheres. The theoretical grids of ionization parameter and chemical abundance are shown in each case.

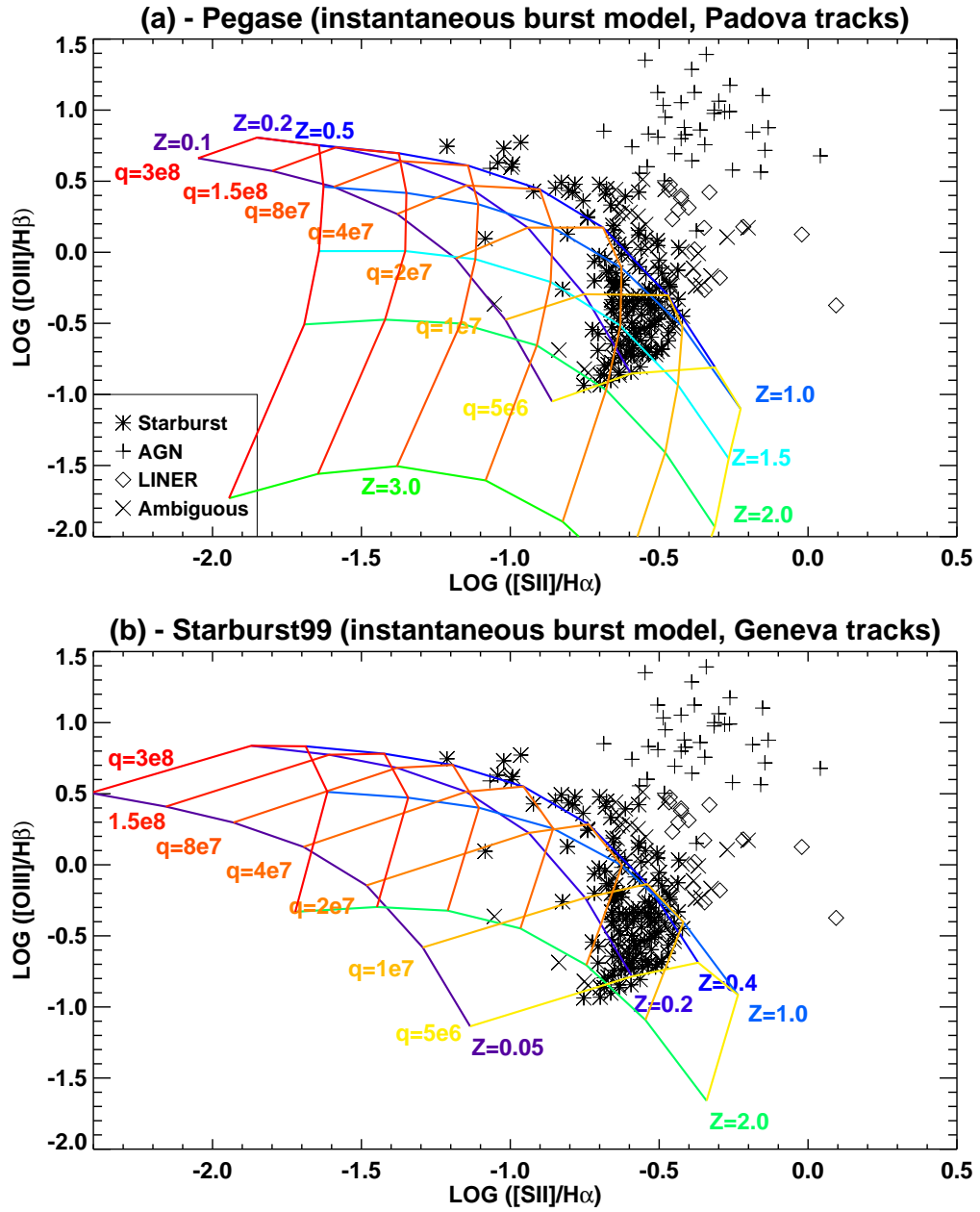


Fig. 5.— As Figure (4) but for the diagram $\log [SII]/H\alpha$ vs $\log [OIII]/H\beta$.

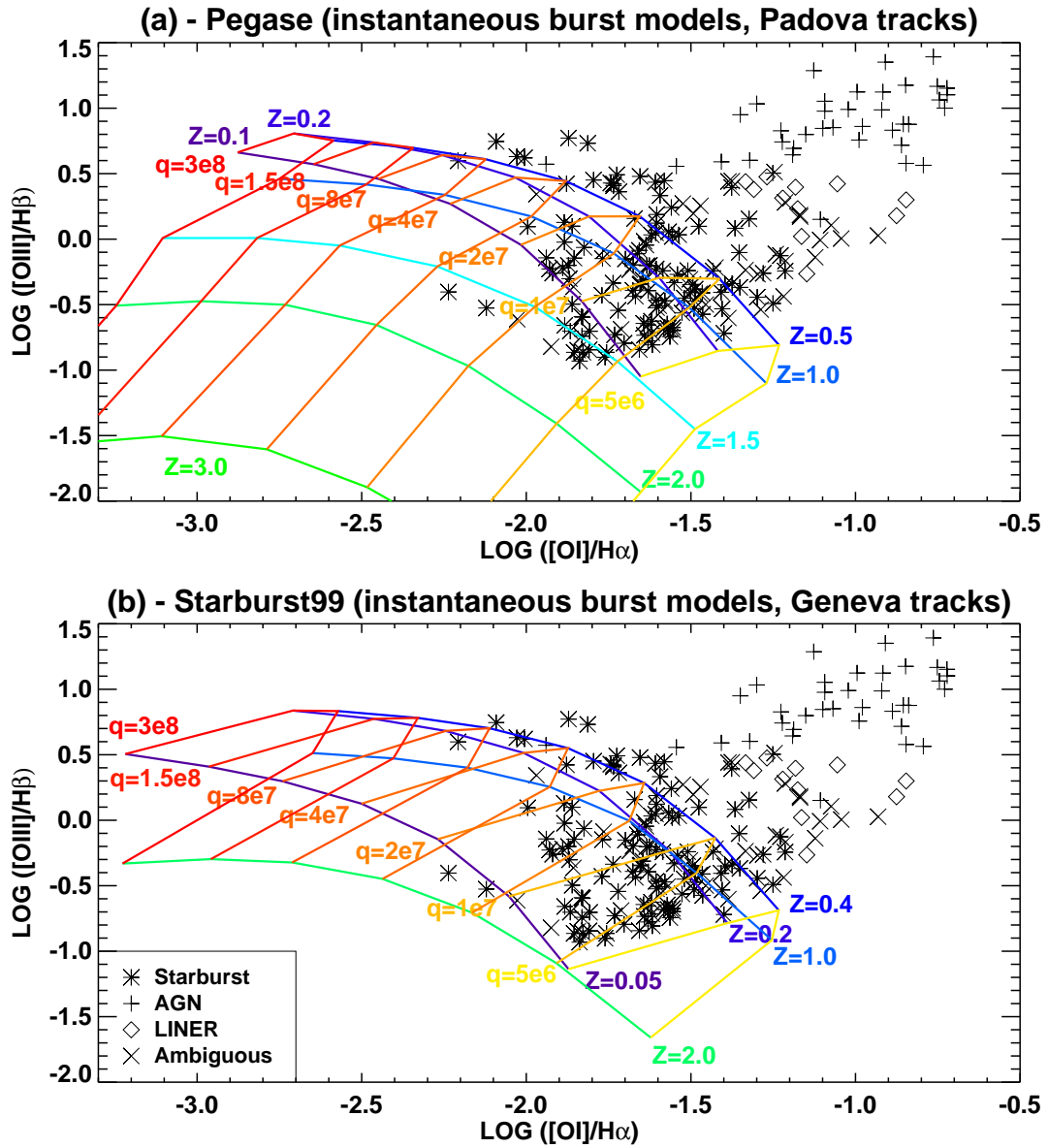


Fig. 6.— As Figure (4) but for the diagram $\log [OI]/H\alpha$ vs $\log [OIII]/H\beta$.

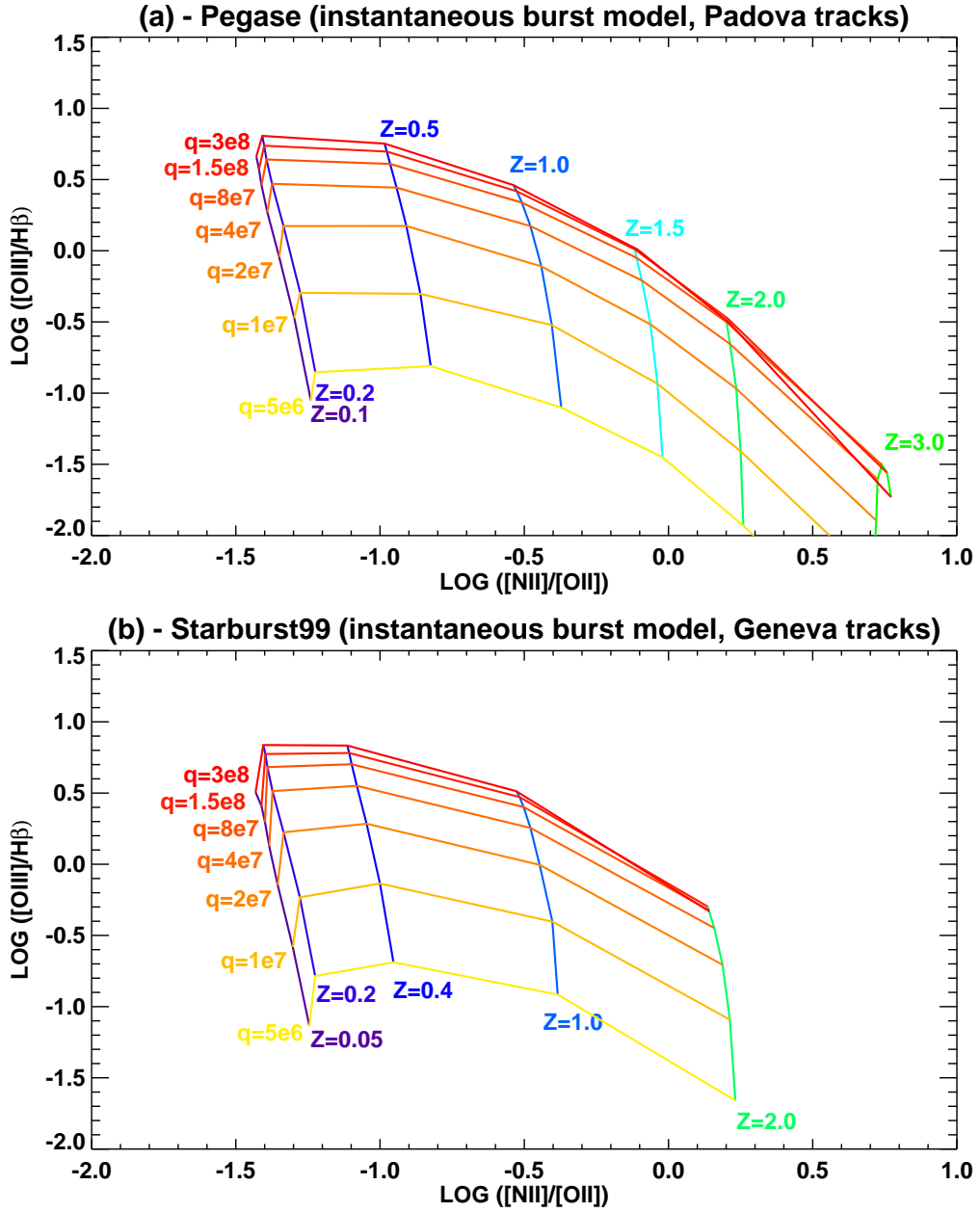


Fig. 7.— As Figure (4) but for the diagram $\log [NII]/[OII]$ vs $\log [OIII]/H\beta$. We do not have $[OII]$ observations for the galaxies in our sample, but we provide this diagram for the use of the astronomical community.

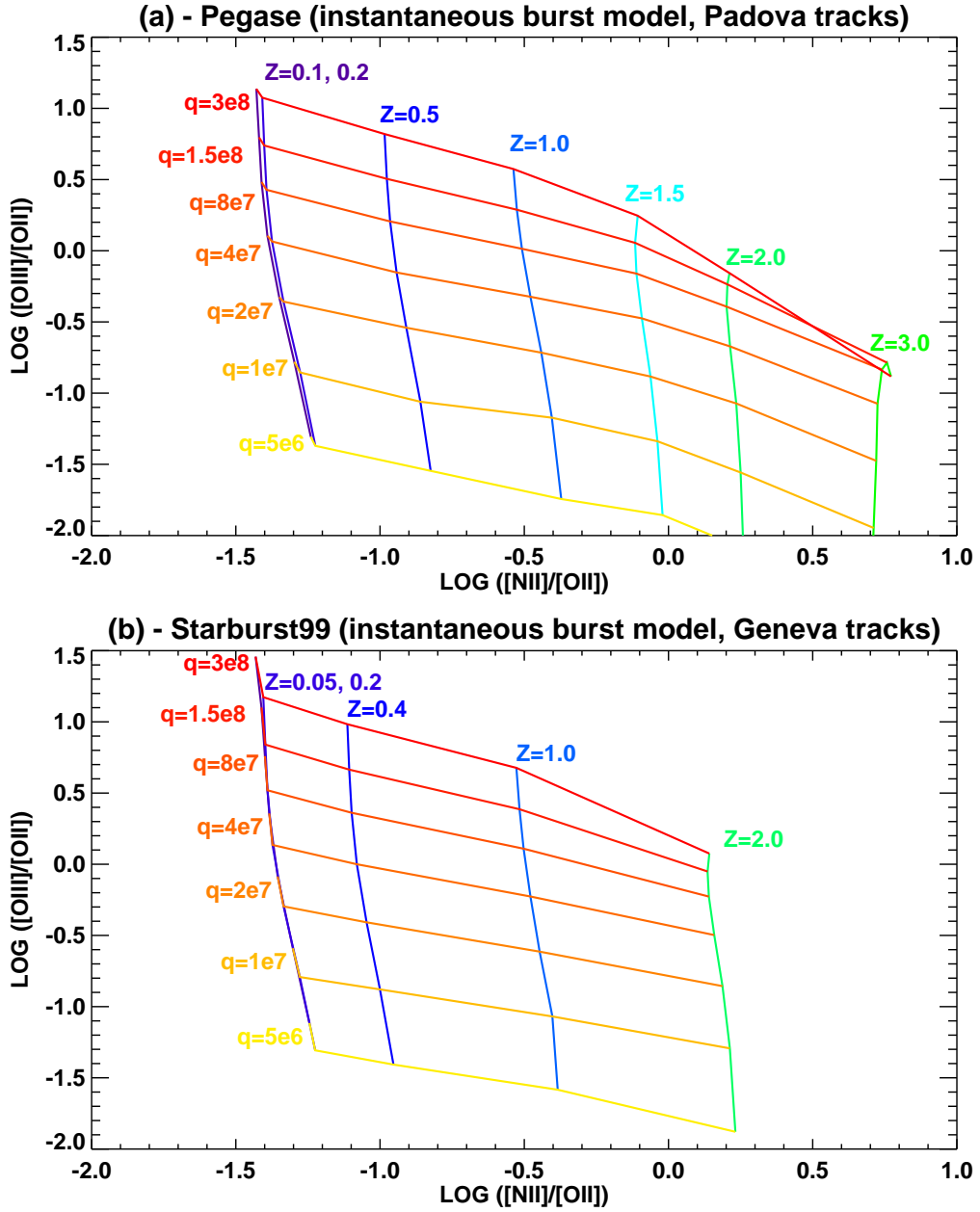


Fig. 8.— As Figure (4) but for the diagram $\log [\text{NII}]/[\text{OII}]$ vs $\log [\text{OIII}]/[\text{OII}]$. We do not have $[\text{OII}]$ observations for the galaxies in our sample, but we provide this diagram for the use of the astronomical community.

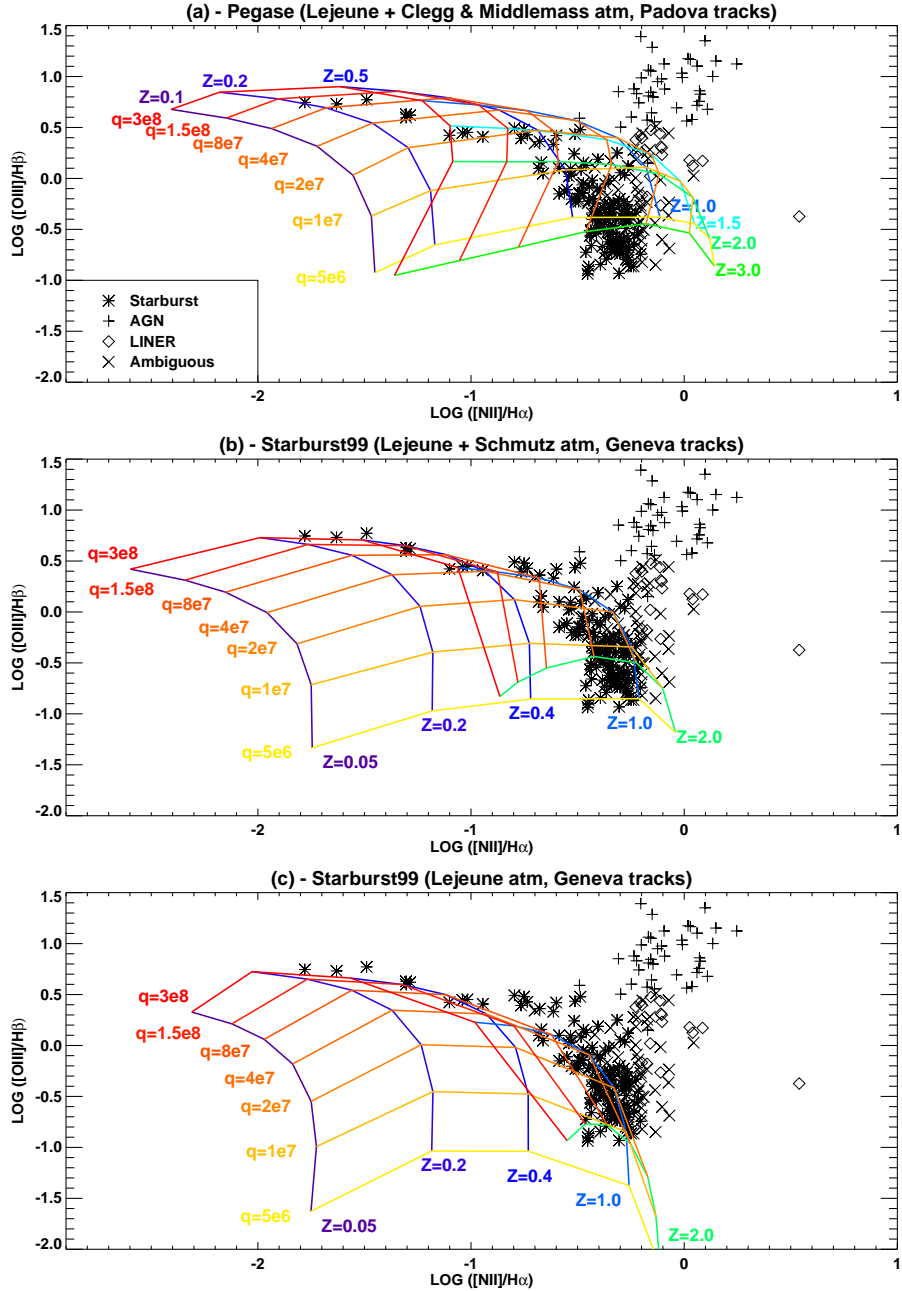


Fig. 9.— The Veilleux & Osterbrock (1987) diagnostic plot $\log [\text{NII}]/\text{H}\alpha$ vs $\log [\text{OIII}]/\text{H}\beta$ for (a) the continuous starburst models based on the PEGASE spectral energy distribution, (b) continuous starburst models based on the STARBURST99 spectral energy distribution with Lejeune plus Schmutz atmospheres, and (c) continuous starburst models based on the STARBURST99 spectral energy distribution with Lejeune atmospheres. The theoretical grids of ionization parameter and chemical abundance are shown in each case.

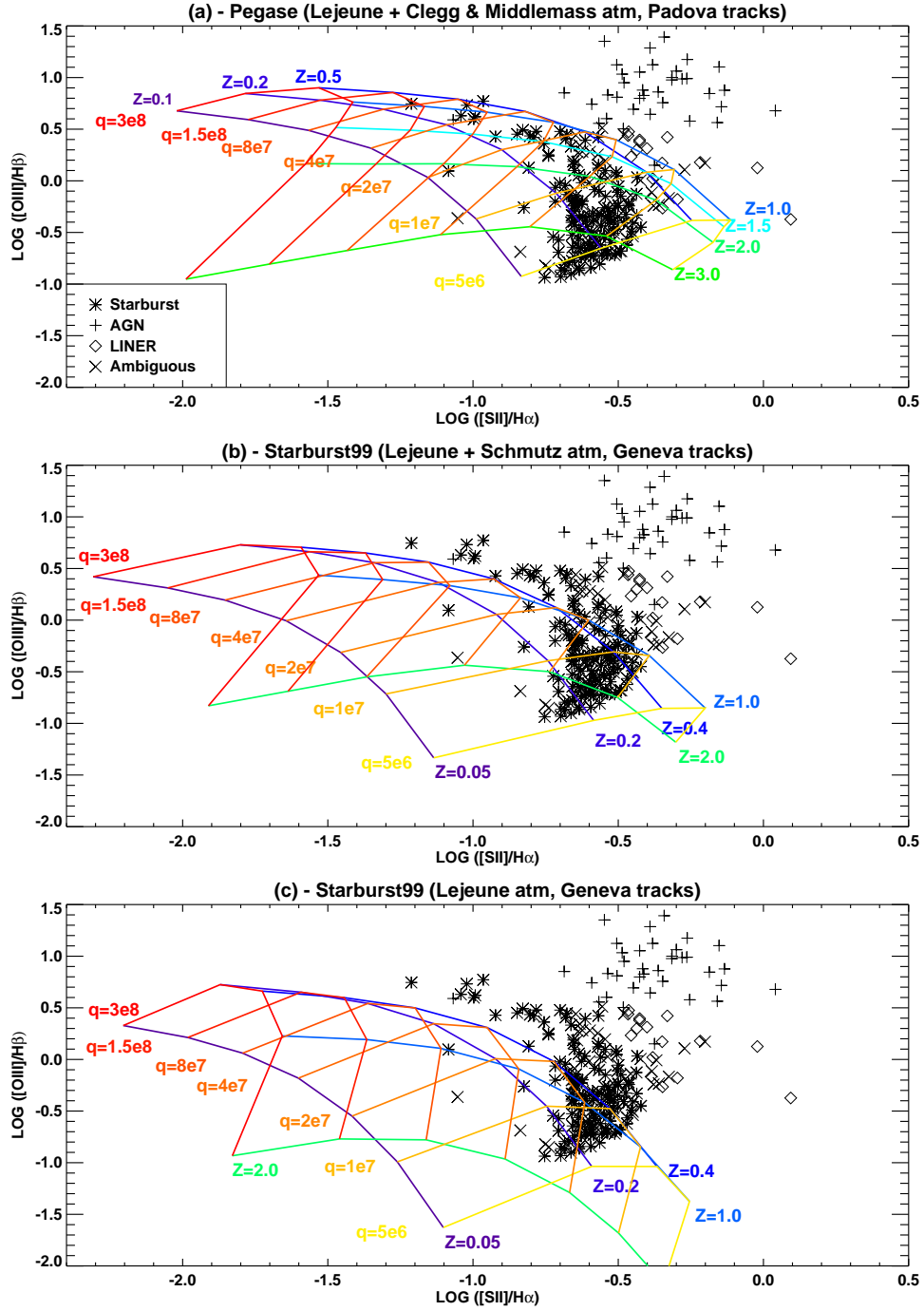


Fig. 10.— As Figure (9) but for the plot $\log [SII]/H\alpha$ vs $\log [OIII]/H\beta$.

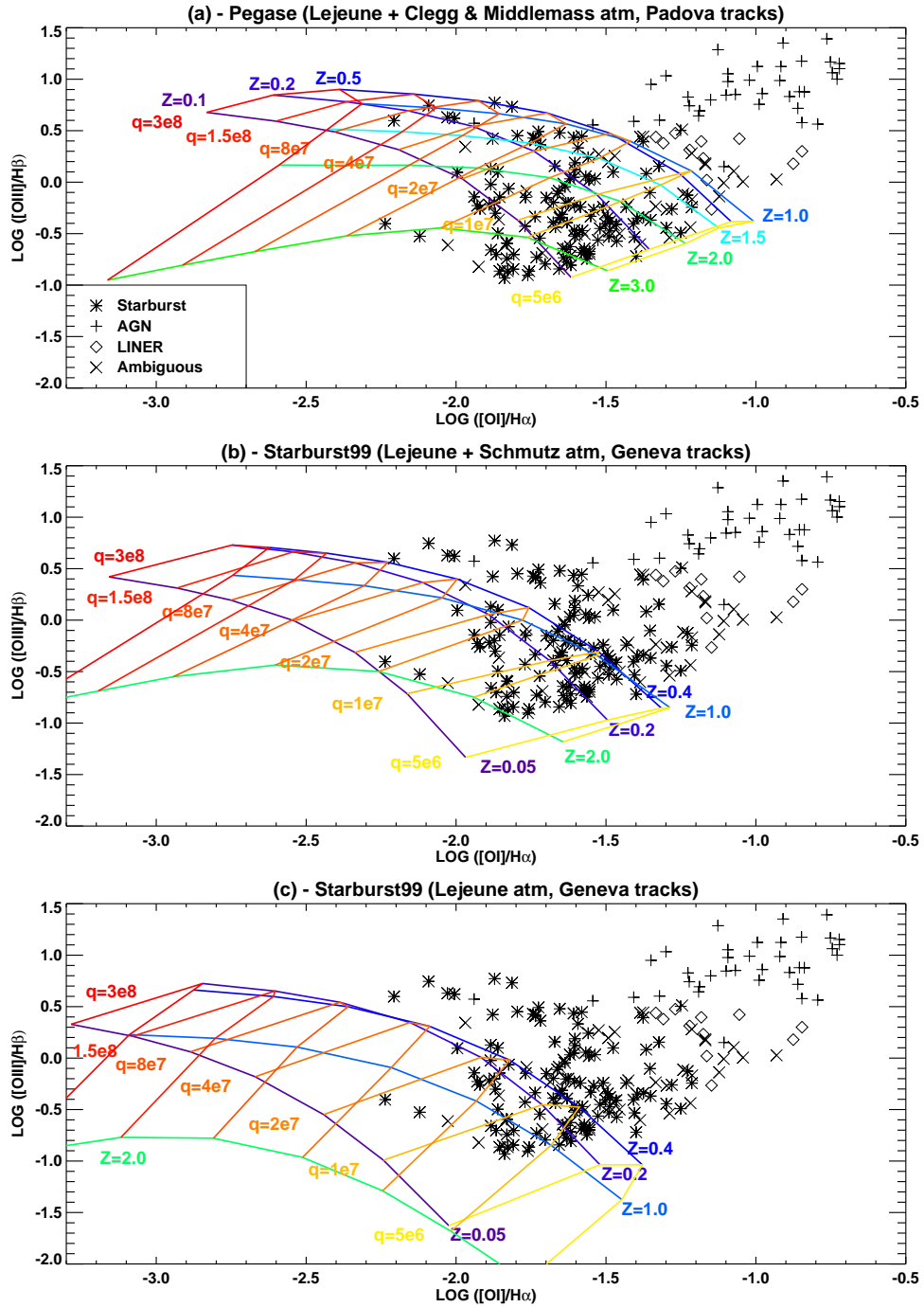


Fig. 11.— As Figure (9) but for the plot $\log [\text{OI}]/\text{H}\alpha$ vs $\log [\text{OIII}]/\text{H}\beta$.

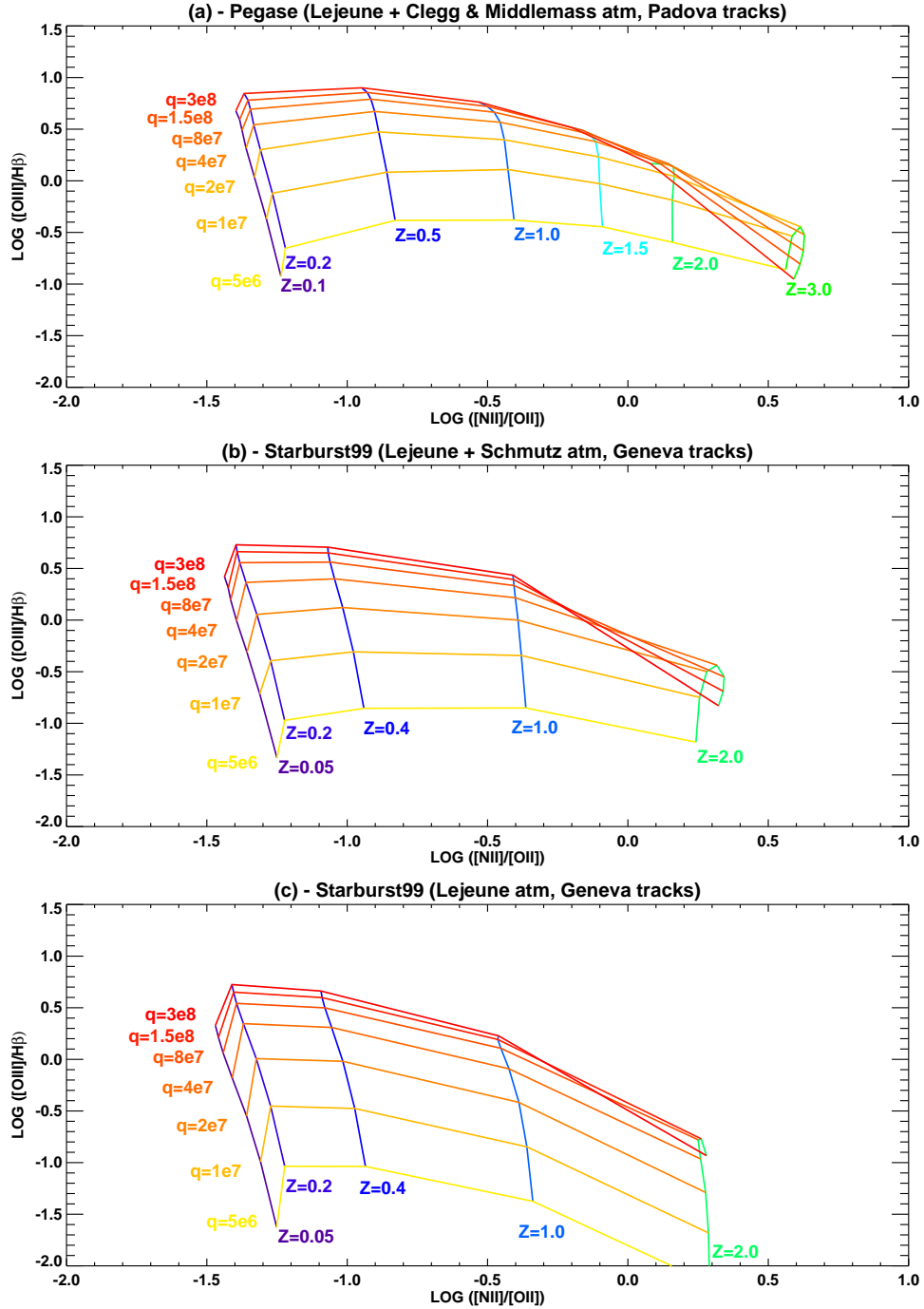


Fig. 12.— As Figure (9) but for the diagram $\log [NII]/[OII]$ vs $\log [OIII]/H\beta$. We do not have $[OII]$ observations for the galaxies in our sample, but we provide this diagram for the use of the astronomical community.

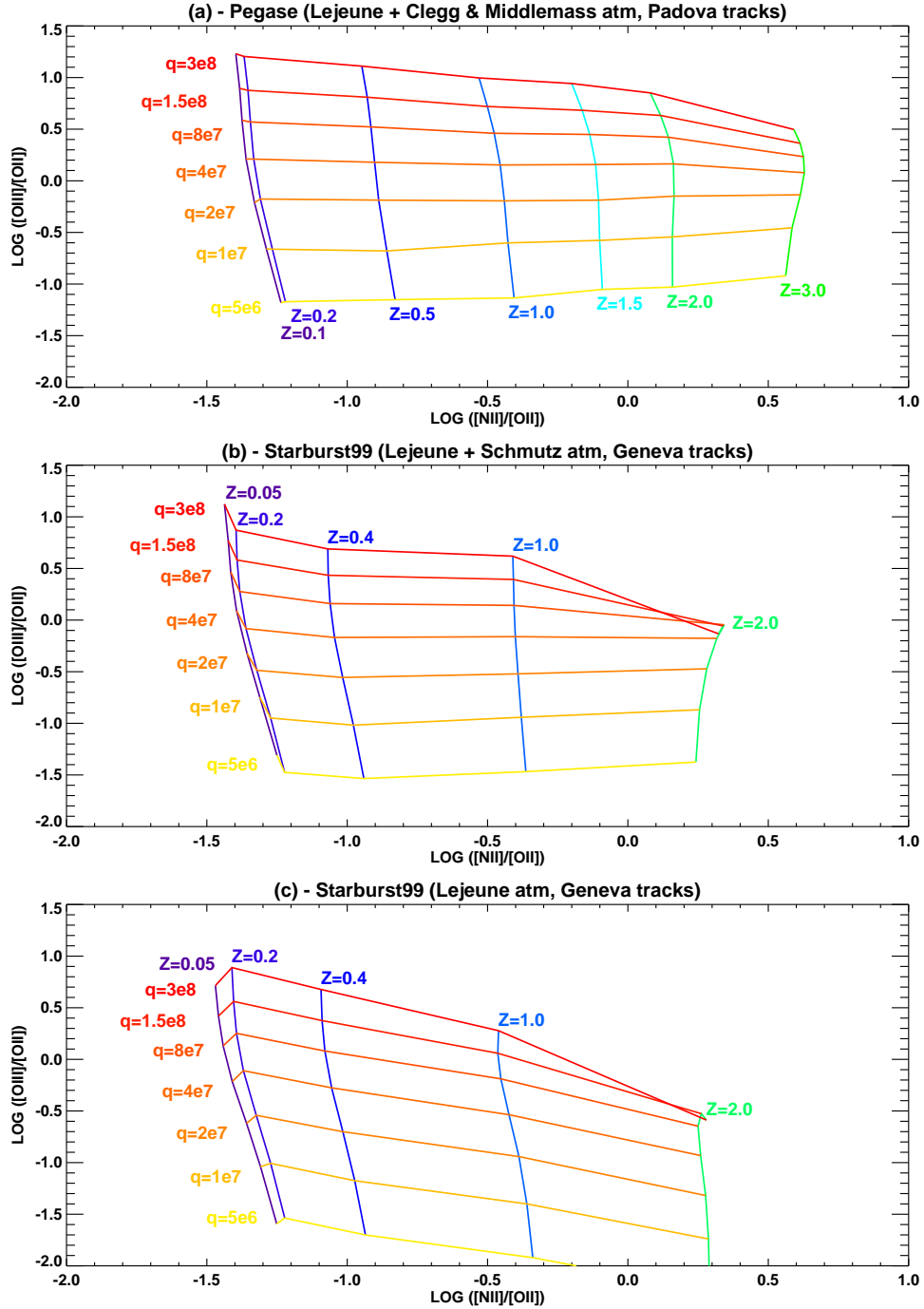


Fig. 13.— As Figure (9) but for the diagram $\log [\text{NII}]/[\text{OII}]$ vs $\log [\text{OIII}]/[\text{OII}]$. We do not have $[\text{OII}]$ observations for the galaxies in our sample, but we provide this diagram for the use of the astronomical community.

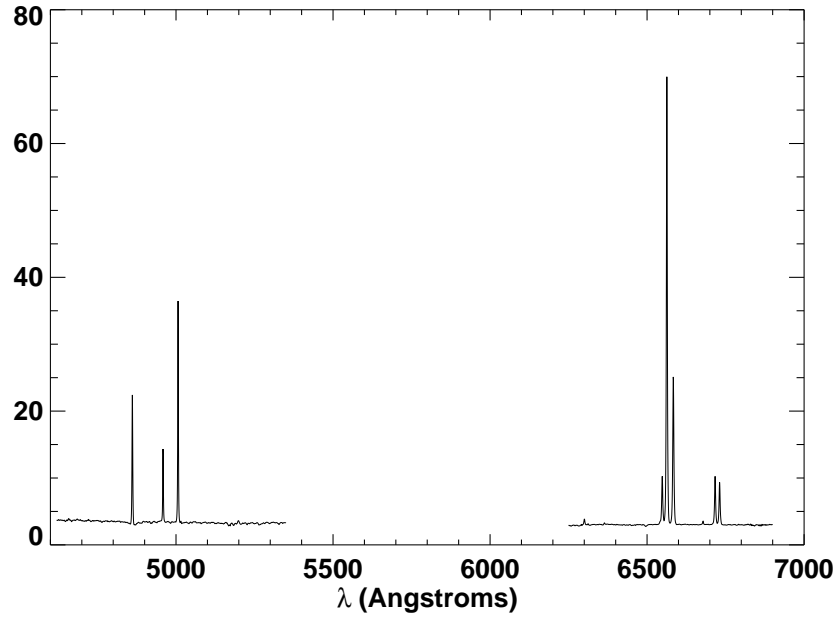


Fig. 14.— Average spectrum of 56 starbursts in our sample which have SNRs greater than 60 at $H\beta$, and zero-redshift blue wavelength cut-off of $\lambda 4620$. Flux is in units of 1×10^{-15} ergs/s/cm²/Å

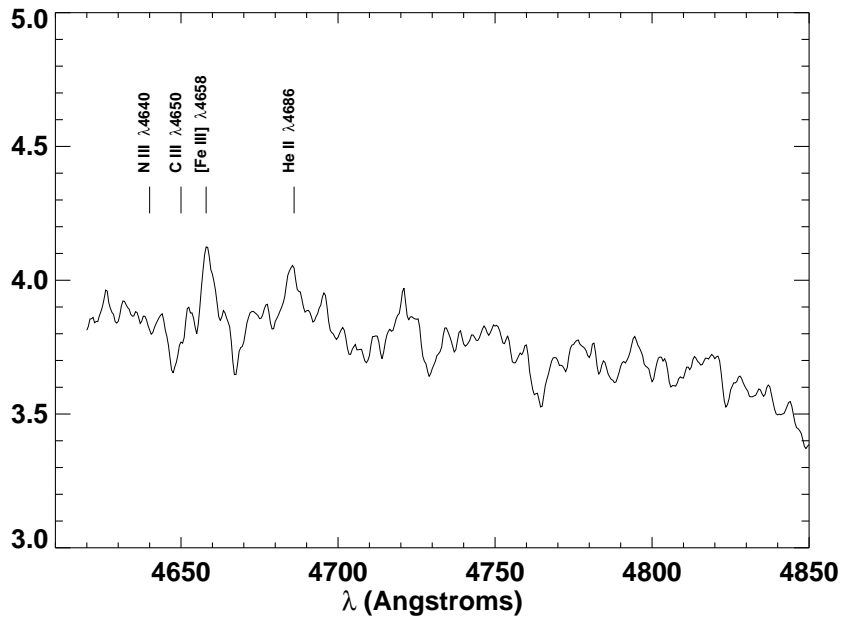


Fig. 15.— Close-up of Figure (14) showing where one would expect to see Wolf-Rayet emission features.

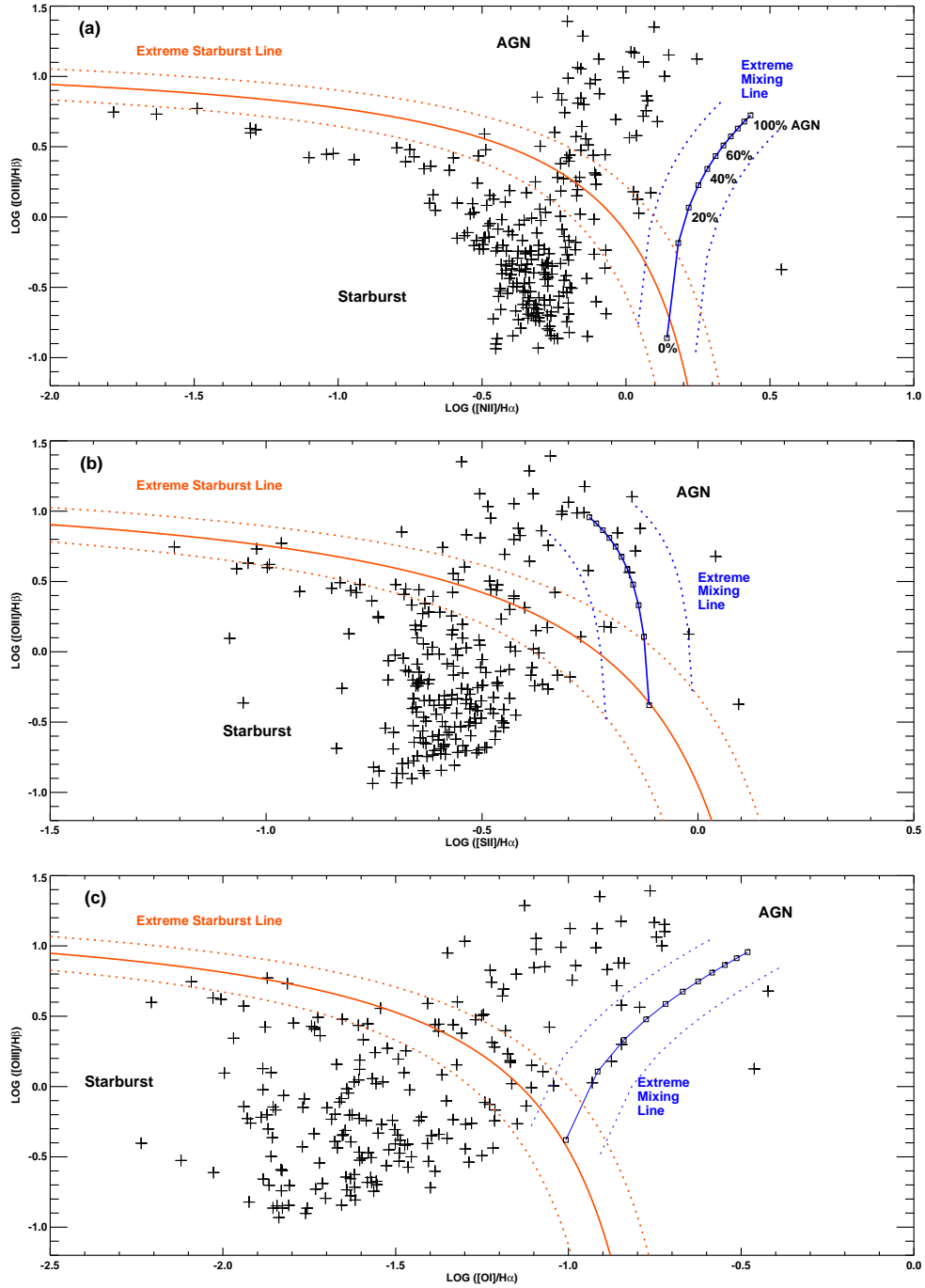


Fig. 16.— Diagnostic diagrams showing the galaxies in our sample. Our theoretical classification line and extreme mixing line are shown in bold, dashed lines represent ± 0.1 dex of these lines, indicating the error range of our modeling.

Table 1. Solar metallicity (Z_{\odot}) and depletion factors (D) adopted for each element.

Element	$\log(Z_{\odot})$	$\log(D)$
H	0.00	0.00
He	-1.01	0.00
C	-3.44	-0.30
N	-3.95	-0.22
O	-3.07	-0.22
Ne	-3.91	0.00
Mg	-4.42	-0.70
Si	-4.45	-1.00
S	-4.79	0.00
Ar	-5.44	0.00
Ca	-5.64	-2.52
Fe	-4.33	-2.00

Table 2. Luminosity expected from a 600 km/s shock with a spherical precursor of 1pc.

Species	L (erg/s)
[O III]	2.5×10^{39}
H β	3.3×10^{38}
H α	9.8×10^{40}